EMVA Standard 1288

Standard for Characterization of Image Sensors and Cameras

Release 4.0 Linear
16 June 2021

Issued by
European Machine Vision Association
www.emva.org

Preface

This document describes Release 4.0 Linear of the EMVA standard 1288 hosted by the European Machine Vision Association (EMVA). This release supersedes Release 3.1 [12], entered into force on December 30, 2016. The EMVA 1288 standard is endorsed by the G3, an initiative for global coordination of machine vision standards.[1] As it is the case with all G3 standards, this document is publicly available free of charge.

Rights, Trademarks, and Licenses

The EMVA holds the intellectual property of the EMVA 1288 standard[2] and owns the "EMVA, standard 1288 compliant" logo. Any company or institution can obtain a license to use the "EMVA standard 1288 compliant" logo, free of charge, with product specifications measured and presented according to the definitions in EMVA standard 1288.

The licensee guarantees that he meets the terms of use in the relevant release of EMVA standard 1288. Licensed users will self-certify compliance of their measurement setup, computation and representation with which the "EMVA standard 1288 compliant" logo is used. The licensee has to check regularly compliance with the relevant release of EMVA standard 1288. For further details, especially the disclosure of any Intellectual Property right claims under control of the licensee with respect to EMVA standard 1288, and how to apply for a

[1] Coorperation agreement on global coordination of machine vision standards, signed on November 3, 2009. Current G3 members include the Automated Imaging Association (AIA), the Chinese Machine Vision Unit (CMVU), the EMVA, the Japanese Industrial Imaging Association (JIIA), and the Mechanical Engineering Industry Association (VDMA).

[2] G3 agreement, §1 preamble, section "Intellectual property"

license please visit the web page of the EMVA at `https://www.emva.org/` in the standards menu.

Anybody publishing data claimed to be EMVA standard 1288 compliant or provides them to a customer or any third party also has to provide the *full datasheet*.[3] An EMVA 1288 compliant datasheet must contain all mandatory measurements and graphs (Table 1) and the standardized EMVA 1288 summary datasheet (see Section 10.2).

EMVA will not be liable for specifications not compliant with the standard and damage resulting therefrom. EMVA keeps the right to withdraw the granted license if a licensee violates one the license rules.

About this Standard

EMVA has started the initiative to define a unified method to measure, compute and present specification parameters and characterization data for cameras and image sensors used for machine vision applications. The standard does not define what nature of data should be disclosed. It is up to the publisher of the datasheet to decide if he wishes to publish typical data, data of an individual component, guaranteed data, or even guaranteed performance over life time of the component. However it shall clearly be indicated what the nature of the presented data is.

The standard includes *mandatory* measurements which must be performed and reported in the datasheet to be EMVA1288 compliant. Further there are *optional* sections which may be skipped for a component where the respective data is not relevant or applicable. It may be necessary to indicate additional, component specific information, not defined in the standard, to better describe the performance of image sensor or camera products, or to describe properties not covered by the standard. It is possible in accordance with the EMVA1288 standard to include such data in the same datasheet. However the data obtained by procedures not described in the current release must be clearly marked as extra measurements not included in the EMVA 1288 standard.

The standard is intended to provide a concise definition and clear description of the measurement process and to benefit the vision industry by providing fast, comprehensive and consistent access to specification information for cameras and sensors. It will be particularly beneficial for those who wish to compare cameras or who wish to calculate system performance based on the performance specifications of an image sensor or a camera.

Starting with Release 4, the EMVA 1288 standard includes two separate documents. This document describes *Release 4 Linear* and is a direct successor of *Release 3.1* [12] with a few changes and extensions. Release 4 Linear, as the name says, is limited to cameras and image sensors with a linear response (characteristic curve). Together with the photon transfer curve, the basic mean parameters temporal dark noise, system gain and quantum efficiencies can be determined.

The separate document *Release 4 General* can be used for much wider classes of cameras and image sensors. It no longer relies on a linear characteristic curve or that raw data are provided. The photon transfer curve is no longer used. The essential point is that basically the same measurements are performed, but they are analyzed in a different way providing still all important application relevant parameters.

While the previous releases of the standard focused on monochrome cameras with a single channel and additionally only included color cameras, Release 4 takes into account the significant advance of multimodal imaging, including polarization, multispectral and time-of-flight (depth imaging). Each of these multimodal sensors includes multiple channels. If the raw data from these channels is available, each channel can be characterized with EMVA 1288 measurements. Polarization imaging serves as a model how the rich tool set of the standard can also be applied to parameters, computed from several channels, here the degree of polarization and the angle of (partially) polarized light.

[3] Either online, on request or in justified exceptions, e. g., for an engineering sample or a product in development, with an NDA. This is a question of research integrity. Results must be recorded in such a way that they "allow verification and replication by others" (Singapore Statement on Research Integrity, 2010, `https://wcrif.org/guidance/singapore-statement`

Acknowledgements

Industry-driven standardization work depends on the personal initiative of the supporting companies' and institutions' delegates as well as from the support of these organizations. The EMVA gratefully acknowledges all contributions to this release of the EMVA standard 1288 (see Appendix F) in the name of the whole vision community.

Contents

Part IV: Appendices

1 Introduction and Scope

As already indicated in the preface, this release of the standard covers all digital cameras with linear photo response characteristics. It is valid for area scan and line scan cameras. Analog cameras can be described according to this standard in conjunction with a frame grabber; similarly, image sensors can be described as part of a camera. If not specified otherwise, the term camera is used for all these items.

1.1 Structure of Document

The standard text is parted into four sections describing the mathematical model and parameters that characterize cameras and sensors with respect to

- Section 2: linearity, sensitivity, and noise for monochrome and color cameras,
- Section 3: dark current,
- Section 4: sensor array nonuniformities and characterization of defect pixels,

a section with an overview of the required measuring setup (Section 5), and five sections that detail the requirements for the measuring setup and the evaluation methods for

- Section 6: linearity, sensitivity, and noise,
- Section 7: dark current,
- Section 8: sensor array nonuniformities and characterization of defect pixels,
- Section 9: spectral sensitivity,

The detailed setup is not regulated in order not to hinder progress and the ingenuity of the implementers. It is, however, mandatory that the measuring setups meet the properties specified by the standard. Section 10 finally describes how to produce the EMVA 1288 datasheets.

Appendix B describes the notation and Appendices C–E details the changes to previous releases [10–12] followed by the list of contributors in Appendix F and a template of the summary datasheet (Appendix G).

1.2 General Assumptions

It is important to note that Release 4 Linear can only be applied if the camera under test can actually be described by the linear model on which it is based. If these conditions are not fulfilled, the computed parameters are meaningless with respect to the camera under test and thus the standard cannot be applied. The general assumptions include

1. The amount of photons collected by a pixel depends on the irradiance $E(t)$ (units $\mathrm{W/m^2}$) at the image plane integrated over the exposure time t_{exp} (units s), i. e., the radiant exposure
$$H = \int_0^{t_{\mathrm{exp}}} E(t)\,\mathrm{d}t \tag{1}$$
at the sensor plane.
2. The sensor is linear, i. e., the digital signal y increases linearly with the number of photons received.
3. The temporal noise at one pixel is statistically independent from the noise at all other pixels. Also the temporal noise in one image is statistically independent from the noise in the next image. The parameters describing the noise are invariant with respect to time and space. All this implies that the power spectrum of the noise is flat both in time and space ("white noise"). If any preprocessing takes place, which breaks this condition, Release 4 Linear cannot be used. Typical examples include debayering, denoising, and edge sharpeing.
4. Temporal noise includes only dark noise and photon shot noise. Therefore Release 4 Linear cannot be applied to intensified and electron multiplying cameras (EM CCD, [4, 5]).

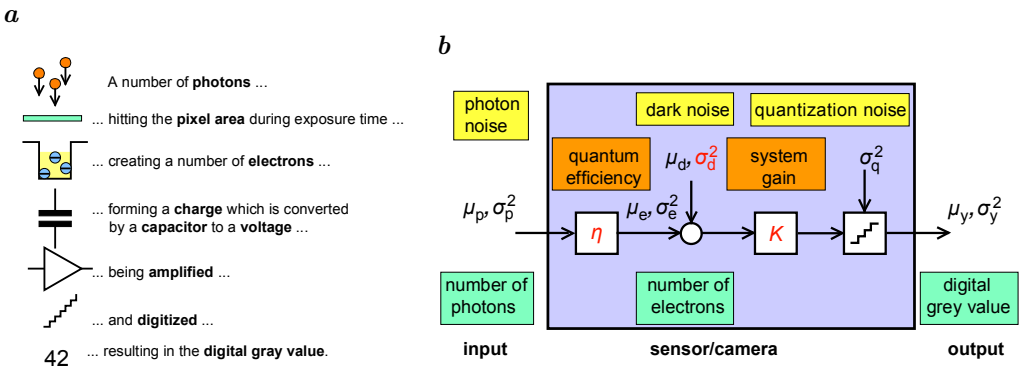

Figure 1: ***a*** *Physical model of the camera and* ***b*** *Mathematical model of a single pixel. Figures separated by comma represent the mean and variance of a quantity; unknown model parameters are marked in red.*

5. Only the total quantum efficiency is wavelength dependent. The effects caused by light of different wavelengths can be linearly superimposed.
6. One photon generates at most one charge unit. Therefore cameras cannot be measured using Release 4 Linear in the deep ultraviolet, where more than one electron per absorbed photon is generated [15]. There is no such limitation to longer wavelengths. Therefore, SWIR sensors can also be measured.
7. Only the dark current is temperature dependent.

These assumptions describe the properties of an *ideal* camera or sensor. A real sensor will depart more or less from an ideal sensor. As long as the deviation is small, the description is still valid and it is one of the tasks of the standard to describe the degree of deviation from an ideal behavior. However, if the deviation is too large, the parameters derived may be too uncertain or may even be rendered meaningless. Then the camera cannot be characterized using Release 4 Linear and Release 4 General must be used.

2 Sensitivity, Linearity, and Noise

This section describes how to characterize the sensitivity, linearity, and temporal noise of a linear image sensor or camera [6, 13, 14, 17].

2.1 Pixel Exposure and Linear Signal Model

As illustrated in Fig. 1, a digital image sensor essentially converts photons hitting the pixel area during the exposure time, into a digital number by a sequence of steps. During the exposure time on average μ_p photons with a wavelength λ hit the whole area A of a single pixel. A fraction

$$\eta(\lambda) = \frac{\mu_e}{\mu_p} \tag{2}$$

of them, the *total quantum efficiency*, is absorbed and accumulates μ_e charge units.[4] The total quantum efficiency as defined here refers to the total area occupied by a single sensor element (pixel) not only the light sensitive area. Consequently, this definition includes the effects of fill factor and microlenses. As expressed in Eq. (2), the quantum efficiency depends on the wavelength of the photons irradiating the pixel.

The mean number of photons that hit a pixel with the area A during the exposure time t_{exp} can be computed from the irradiance E on the sensor surface in W/m^2 by

$$\mu_p = \frac{AEt_{\text{exp}}}{h\nu} = \frac{AEt_{\text{exp}}}{hc/\lambda}, \tag{3}$$

[4] The actual mechanism is different for CMOS sensors, however, the mathematical model for CMOS is the same as for CCD sensors

using the well-known quantization of the energy of electromagnetic radiation in units of $h\nu$. With the values for the speed of light $c = 2.99792458 \cdot 10^8$ m/s and Planck's constant $h = 6.6260755 \cdot 10^{-34}$ Js, the photon irradiance is given in handy units for image sensors by

$$\mu_p[\text{photons}] = 50.34 \cdot A[\mu\text{m}^2] \cdot t_{\text{exp}}[\text{ms}] \cdot \lambda[\mu\text{m}] \cdot E\left[\frac{\mu\text{W}}{\text{cm}^2}\right]. \tag{4}$$

This equation is used to convert the irradiance E at the sensor plane calibrated by radiometers in units of W/cm^2 into the quantum exposure μ_p required to characterize image sensors.

In the camera electronics, the charge units accumulated by the photo irradiance is converted into a voltage, amplified, and finally converted into a digital signal y by an analog digital converter (ADC). The whole process is assumed to be linear and can be described by a single quantity, the *overall system gain* K with units DN/e$^-$, i. e., digits per electrons.[5] Then the mean digital signal μ_y results in

$$\mu_y = K(\mu_e + \mu_d) \quad \text{or} \quad \mu_y = \mu_{y.\text{dark}} + K\mu_e, \tag{5}$$

where μ_d is the mean number electrons present without light, which result in the mean dark signal $\mu_{y.\text{dark}} = K\mu_d$ in units DN with zero radiant exposure. Note that the dark signal will generally depend on other parameters, especially the exposure time and the ambient temperature (Section 3).

With Eqs. (2) and (3), Eq. (5) results in a linear relation between the mean gray value μ_y and the number of photons irradiated during the exposure time onto the pixel:

$$\boxed{\mu_y = \mu_{y.\text{dark}} + K\eta\,\mu_p = \mu_{y.\text{dark}} + K\eta\frac{\lambda A}{hc}\,E\,t_{\text{exp}}.} \tag{6}$$

This equation can be used to verify the linearity of the sensor by measuring the mean gray value in relation to the mean number of photons incident on the pixel and to measure the *responsivity* $R = K\eta$ from the slope of the relation. Once the overall system gain K is determined from Eq. (15), it is also possible to estimate the quantum efficiency from the responsivity $K\eta$.

2.2 Description of Polarized Light

For the measurement of polarization cameras or to test whether a normal camera shows any polarization-dependent effects, linear polarized light is required. Circular polarized light is not yet considered, because currently no imaging sensors are available which can detect circular polarized light.

Without consideration of circular polarization, polarized light can be described by the first three Stokes components [26, Sec. 6.1], which can be measured with linear polarized light oriented in the four directions 0, 45, 90, and 135 degrees and with the irradiances E_0, E_{45}, , E_{90}, and E_{135}:

$$\begin{bmatrix} S_0 \\ S_1 \\ S_2 \end{bmatrix} = \begin{bmatrix} E_0 + E_{90} \\ E_0 - E_{90} \\ E_{45} - E_{135} \end{bmatrix}. \tag{7}$$

From the Stokes components, the following three parameters can be derived, which are required for imaging applications with polarized light:

- *Total irradiance* is simply the first component S_0, which can be determined from two radiant exposures using linear polarized light perpendicular to each other.
- *Linear degree of polarization* is given by:

$$P = \frac{\sqrt{S_1^2 + S_2^2}}{S_0}. \tag{8}$$

- *Polarization angle* gives the orientation of partially linear polarized light:

$$\alpha = \arctan(S_2/S_1). \tag{9}$$

[5] DN is a dimensionless unit, but for sake of clarity, it is better to denote it specifically.

2.3 Polarization Properties of a Polarization Camera

A polarization camera contains J channels of images denoted by $\boldsymbol{y}_j$. Each channel has a linear polarizer in a given direction. For each channel the quality of the polarizing sensor elements must be analyzed. This includes the following three properties: response, orientation of the linear polarizer, and the polarization quality. For the latter, the best parameter is not the *degree of linear polarization* P, because this is a number close to 1, but $1 - P$, which is also the inverse of the *extinction ratio* [26, Sec. 6.1].

Because three unknowns must be determined, one illumination with linear polarized light with just one orientation is not sufficient. At least three orientations are required, but an even number of $Q \geq 4$ orientation steps with a step increment of $180/Q$ should be used, because then perpendicular polarization orientations are gained. The response of the polarization filter of channel j to the exposure with polarization state q be $\boldsymbol{y}_{jq}$ (an averaged dark image must be subtracted) and is modeled by

$$\boldsymbol{y}_{jq} = \boldsymbol{y}_j \left[1 - \boldsymbol{P}_j + \frac{\boldsymbol{P}_j}{2} + \frac{\boldsymbol{P}_j}{2} \cos 2(\boldsymbol{\alpha}_j - \alpha_q)\right]. \tag{10}$$

The three unknowns maximum response $\boldsymbol{y}_j$, $1 - \boldsymbol{P}_j$, and polarization angle $\boldsymbol{\alpha}_j$ for each channel j and at each pixel can be computed as follows. Using the following intermediate parameters

$$\begin{aligned} \boldsymbol{a} &= \frac{1}{Q}\sum_{q=0}^{Q-1} \boldsymbol{y}_{jq}, \\ \boldsymbol{r} &= \frac{2}{Q}\sum_{q=0}^{Q-1} \boldsymbol{y}_{jq} \cos(2\pi q/Q), \\ \boldsymbol{s} &= \frac{2}{Q}\sum_{q=0}^{Q-1} \boldsymbol{y}_{jq} \sin(2\pi q/Q), \\ \boldsymbol{m} &= \sqrt{\boldsymbol{r}^2 + \boldsymbol{s}^2} \end{aligned} \tag{11}$$

the three unknowns are given by

$$\boldsymbol{y}_j = \boldsymbol{a} + \boldsymbol{m}, \quad 1 - \boldsymbol{P}_j = \frac{\boldsymbol{a} - \boldsymbol{m}}{\boldsymbol{a} + \boldsymbol{m}}, \quad \boldsymbol{\alpha}_j = \arctan(\boldsymbol{s}/\boldsymbol{r}). \tag{12}$$

For these parameters, it is then possible to compute mean values, temporal variances, and variances of spatial nonuniformity just as for a single image. For details see Section 6.8.

2.4 Noise Model

The number of charge units (electrons) fluctuates statistically. This noise, often referred to as *shot noise* is given by the basic laws of physics and equal for all types of cameras. According to the laws of quantum mechanics, the probability is Poisson distributed. Therefore the variance of the fluctuations is equal to the mean number of accumulated electrons:

$$\sigma_e^2 = \mu_e. \tag{13}$$

All other noise sources depend on the specific construction of the sensor and the camera electronics. Due to the linear signal model (Section 2.1), all noise sources add up. For the purpose of a camera model treating the whole camera electronics as a black box it is sufficient to consider only two additional noise sources. All noise sources related to the sensor read out and amplifier circuits can be described by a signal independent normal-distributed noise source with the variance σ_d^2. The final analog digital conversion (Fig. 1b) adds another noise source that is uniform-distributed between the quantization intervals and has a variance $\sigma_q^2 = 1/12\,\mathrm{DN}^2$ [17].Because the variances of all noise sources add up linearly, the total temporal variance of the digital signal y, σ_y^2, is given according to the laws of error propagation by

$$\sigma_y^2 = K^2\left(\sigma_d^2 + \sigma_e^2\right) + \sigma_q^2 \tag{14}$$

Using Eqs. (13) and (5), the noise can be related to the measured mean digital signal:

$$\boxed{\sigma_y^2 = \underbrace{K^2\sigma_d^2 + \sigma_q^2}_{\text{offset}} + \underbrace{K}_{\text{slope}} (\mu_y - \mu_{y.\text{dark}}).} \tag{15}$$

This equation is central to the characterization of the sensor. From the linear relation between the variance of the noise σ_y^2 and the mean photo-induced gray value $\mu_y - \mu_{y.\text{dark}}$ it is possible to determine the overall system gain K from the slope and the dark noise variance σ_d^2 from the offset. This method is known as the *photon transfer method* [14, 16].

2.5 Computation of mean and variance of measured gray values

For the characteristic or sensitivity curve (Section 2.1, Eq. (6)) and the photon transfer curve (Section 2.4, Eq. (15)) it is required to compute the mean gray values and the temporal variance of the gray values at many exposure steps. This is done in an efficient way using only two images taken at the same radiant exposure in the following way:

Mean gray value. The mean of the gray values μ_y over *all* $M \times N$ pixels in the active area at each exposure level is computed from the two captured $M \times N$ images $\boldsymbol{y}[0]$ and $\boldsymbol{y}[1]$ as

$$\mu_y[k] = \frac{1}{NM} \sum_{m=0}^{M-1} \sum_{n=0}^{N-1} y[k][m][n], \ (k = 0, 1) \quad \text{and} \quad \mu_y = \frac{1}{2}(\mu_y[0] + \mu_y[1]) \tag{16}$$

averaging over M rows and N columns.
In the same way, the mean gray value of dark images, $\mu_{y.\text{dark}}$, is computed.

Temporal variance of gray value. Normally, the computation of the temporal variance would require the capture of many images. However on the assumptions put forward in Section 1.2, the temporal noise is stationary and homogenous and it could also be averaged over the many pixels of a single image. The variance computed in this way from just one image $\boldsymbol{y}[k]$ contains also the spatial variance of the nonuniformity s_y^2 (see Section 4.2)

$$\frac{1}{NM} \sum_{m=0}^{M-1} \sum_{n=0}^{N-1} \left(y[k][m][n] - \mu[0]\right)^2 = \sigma_y^2 + s_y^2. \tag{17}$$

Temporal noise causes the gray values to be different from one image to the next, but the nonuniformity is stationary ("fixed pattern noise"). Therefore the variance of spatial nonuniformity can be eliminated by

$$\begin{aligned} \sigma_y^2 &= \frac{1}{2NM} \sum_{m=0}^{M-1} \sum_{n=0}^{N-1} \left[(y[0][m][n] - \mu[0]) - (y[1][m][n] - \mu[1])\right]^2 \\ &= \frac{1}{2NM} \sum_{m=0}^{M-1} \sum_{n=0}^{N-1} \left(y[0][m][n] - y[1][m][n]\right)^2 - \frac{1}{2}\left(\mu[0] - \mu[1]\right)^2. \end{aligned} \tag{18}$$

Because the variance of the difference of two values is the sum of the variances of the two values, the variance of the temporal noise computed in this way must be divided by two as indicated in Eq. (18).
The correction for the variance σ_y^2 in Eq. (18) by the difference of the mean values of the two images is new in Release 4. It gives an unbiased estimate even if the mean values are slightly different by a temporal noise source that causes all pixels to fluctuate in sync.
The statistical uncertainty of the variance estimation averaged over NM values is according to Papoulis [22, Sec. 8.2] and Jähne [17, Sec. 3.4.4] given by

$$\frac{\sigma(\sigma_y^2)}{\sigma_y^2} = \sqrt{\frac{2}{NM}}. \tag{19}$$

This means that for a megapixel image sensor the standard deviation in the estimation of the temporal variance is about 0.14%.[6]

[6] Therefore it is also justified to use NM in the estimation of the variance and not the correct value $NM - 1$ for an unbiased estimation. This is just a relative difference of 10^{-6} for a megapixel image sensor.

2.6 Signal-to-Noise Ratio (SNR)

The quality of the signal is expressed by the signal-to-noise ratio (SNR), which is defined as

$$\mathrm{SNR} = \frac{\mu_y - \mu_{y.\mathrm{dark}}}{\sigma_y}. \tag{20}$$

Using Eqs. (6) and (14), the SNR can then be written as

$$\boxed{\mathrm{SNR}(\mu_p) = \frac{\eta\mu_p}{\sqrt{\sigma_d^2 + \sigma_q^2/K^2 + \eta\mu_p}}.} \tag{21}$$

Except for the small effect caused by the quantization noise, the overall system gain K cancels out so that the SNR depends only on the quantum efficiency $\eta(\lambda)$ and the dark signal noise σ_d in units e^-. Two limiting cases are of interest: the high-photon range with $\eta\mu_p \gg \sigma_d^2 + \sigma_q^2/K^2$ and the low-photon range with $\eta\mu_p \ll \sigma_d^2 + \sigma_q^2/K^2$:

$$\mathrm{SNR}(\mu_p) \approx \begin{cases} \sqrt{\eta\mu_p}, & \eta\mu_p \gg \sigma_d^2 + \sigma_q^2/K^2, \\ \dfrac{\eta\mu_p}{\sqrt{\sigma_d^2 + \sigma_q^2/K^2}}, & \eta\mu_p \ll \sigma_d^2 + \sigma_q^2/K^2. \end{cases} \tag{22}$$

This means that the slope of the SNR curve changes from a linear increase at low exposure to a slower square root increase at high exposure.

A real sensor can always be compared to an *ideal* sensor with a quantum efficiency $\eta = 1$, no dark noise ($\sigma_d = 0$) and negligible quantization noise ($\sigma_q/K = 0$). The SNR of an ideal sensor is given by

$$\mathrm{SNR}_{\mathrm{ideal}} = \sqrt{\mu_p}. \tag{23}$$

Using this curve in SNR graphs, it becomes immediately visible how close a real sensor comes to an ideal sensor.

2.7 Signal Saturation and Absolute Sensitivity Threshold

For a k-bit digital camera, the digital gray values are in a range between 0 and $2^k - 1$. The practically useable gray value range is smaller, however. The mean dark gray value $\mu_{y.\mathrm{dark}}$ must be higher than zero so that no significant underflow occurs by temporal noise and the dark signal nonuniformity. Likewise the maximal usable gray value is lower than $2^k - 1$ because of the temporal noise and the photo response nonuniformity.

Therefore, the *saturation exposure* $\mu_{p.\mathrm{sat}}$ is defined in such a way that the clipping of the distribution of the digital signal at the saturation exposure is minor so that the computation of both the mean and variance are not biased. For exact definitions see Section 6.5.

From the saturation exposure $\mu_{p.\mathrm{sat}}$ the *saturation capacity* $\mu_{e.\mathrm{sat}}$ can be computed:

$$\boxed{\mu_{e.\mathrm{sat}} = \eta\mu_{p.\mathrm{sat}}.} \tag{24}$$

The saturation capacity must not be confused with the *full-well capacity*. It is normally lower than the full-well capacity, because the signal is clipped to the maximum digital value $2^k - 1$ before the physical saturation of the pixel is reached.

The *minimum detectable exposure* or *absolute sensitivity threshold*, $\mu_{p.\mathrm{min}}$ can be defined by using the SNR. It is the mean number of photons required so that the SNR is equal to 1.

For this purpose, it is required to know the inverse function to Eq. (21), i. e., the number of photons required to reach a given SNR. Inverting Eq. (21) results in

$$\boxed{\mu_p(\mathrm{SNR}) = \frac{\mathrm{SNR}^2}{2\eta}\left(1 + \sqrt{1 + \frac{4(\sigma_d^2 + \sigma_q^2/K^2)}{\mathrm{SNR}^2}}\right).} \tag{25}$$

The absolute sensitivity threshold in units of photons, i. e., $\mu_p(\mathrm{SNR}=1)$ and denoted by $\mu_{p.\min}$ is then given by

$$\mu_{p.\min} = \frac{1}{\eta}\left(\sqrt{\sigma_d^2 + \sigma_q^2/K^2 + 1/4} + \frac{1}{2}\right) = \frac{1}{\eta}\left(\sqrt{\sigma_{y.\mathrm{dark}}^2/K^2 + 1/4} + \frac{1}{2}\right) \geq \frac{1}{\eta}. \tag{26}$$

Note that the absolute sensitivity threshold in units of electrons, $\mu_{e.\min}$, is not equal to σ_d, but a bit higher because of the quantization noise σ_q and the nonlinear SNR curve:

$$\mu_{e.\min} = \left(\sqrt{\sigma_d^2 + \sigma_q^2/K^2 + 1/4} + \frac{1}{2}\right) \geq 1. \tag{27}$$

The ratio of the signal saturation to the absolute sensitivity threshold is defined as the *dynamic range* (DR):

$$\mathrm{DR} = \frac{\mu_{p.\mathrm{sat}}}{\mu_{p.\min}}. \tag{28}$$

3 Dark Current

3.1 Mean and Variance

The dark signal μ_d introduced in the previous section, see Eq. (5), is not constant. The dark signal is mainly caused by thermally induced electrons. Therefore, the dark signal has an offset of $\mu_{d.0}$ (value at zero exposure time) and increases linearly with the exposure time

$$\mu_d = \mu_{d.0} + \mu_{\mathrm{therm}} = \mu_{d.0} + \mu_{I.y} t_{\mathrm{exp}}. \tag{29}$$

In this equation all quantities are expressed in units of electrons (e^-/pixel). These values can be obtained by dividing the measured values in the units DN by the overall system gain K (Eq. (15)). The quantity μ_I is named the *dark current*, given in the units e^-/(pixel s).

According to the laws of error propagation, the variance of the dark signal is then given as

$$\sigma_d^2 = \sigma_{d.0}^2 + \sigma_{\mathrm{therm}}^2 = \sigma_{d.0}^2 + \mu_{I.e} t_{\mathrm{exp}}, \tag{30}$$

because the thermally induced electrons are Poisson distributed as are the light induced ones in Eq. (13) with $\sigma_{\mathrm{therm}}^2 = \mu_{\mathrm{therm}}$. If a camera or sensor has a dark current compensation, the dark current can only be characterized using Eq. (30).

3.2 Temperature Dependence

Because of the thermal generation of charge units, the dark current increases roughly exponentially with the temperature [13, 15, 27]. In Release 3.1 this was expressed by

$$\mu_I = \mu_{I.\mathrm{ref}} \cdot 2^{(T - T_{\mathrm{ref}})/T_d}. \tag{31}$$

The constant T_d has units K or ^{o}C and indicates the temperature interval that causes a doubling of the dark current. The temperature T_{ref} is a reference temperature at which all other EMVA 1288 measurements are performed and $\mu_{I.\mathrm{ref}}$ the dark current at the reference temperature. Many modern CMOS sensors no longer show such a simple exponential increase of the dark current. Therefore in Release 4 a specific model about the temperature increase of the dark current is no longer assumed. Only the data are presented.

The measurement of the temperature dependency of the dark current is the only measurement to be performed at different ambient temperatures, because it is the only camera parameter with a *strong* temperature dependence.

4 Spatial Nonuniformity and Defect Pixels

The model discussed so far considered only a single or average pixel. All parameters of an array of pixels, will however vary from pixel to pixel. Sometimes these nonuniformities are

called *fixed pattern noise*, or *FPN*. This expression is however misleading, because inhomogeneities are not noise that makes the signal vary in time. The inhomogeneity may only be distributed randomly. Therefore it is better to name this effect *nonuniformity*.

For a linear sensor there are only two basic nonuniformities. The characteristic curve can have a different offset and different slope for each pixel. The dark signal varying from pixel to pixel is called *dark signal nonuniformity*, abbreviated to *DSNU*. The variation of the sensitivity is called *photo response nonuniformity*, abbreviated to *PRNU*. The spatial variations of the dark current, the *dark current nonuniformity*, or *DCNU* and the *full-well capacity* are not yet covered by the EMVA standard 1288.

4.1 Types of Nonuniformities

Spatial nonuniformities are more difficult to describe than temporal noise because they are not just random. For an adequate description, several effects must be considered:

Gradual variations. Manufacturing imperfections can cause gradual low-frequency variations over the whole chip. This effect is not easy to measure because it requires a very homogeneous irradiation of the chip, which is difficult to achieve. Fortunately this effect does not really degrade the image quality significantly. A human observer does not detect it at all and additional gradual variations are introduced by lenses (shading, vignetting) and nonuniform illumination. Therefore, gradual variations must be corrected with the complete image system anyway for applications that demand a flat response over the whole sensor array.

Periodic variations and spatial patterns. This type of distortion is very nasty, because the human eye detects such distortions very sensitively, especially if there are column and row patterns. Likewise many image processing operations are disturbed.

Outliers. These are single pixels or cluster of pixels that show a significant deviation from the mean.

Random variations. If the spatial nonuniformity is purely random, i. e., shows no spatial correlation, the power spectrum is flat, i. e., the variations are distributed equally over all wave numbers. Such a spectrum is called a *white spectrum*. The outlier pixels also contribute to a flat spectrum.

The EMVA 1288 standard describes nonuniformities in four different ways. The variance of spatial nonuniformity (Section 4.2) and the split into column, row, and pixel variances (Sections 4.3 and 8.2), , introduced in Release 4, are a simple overall measure of the spatial nonuniformity including horizontal and vertical patterns. The spectrogram method, i. e., a power spectrum of the spatial variations (Section 8.6), offers a way to analyze patterns or periodic spatial variations. In the spectrogram, periodic variations show up as sharp peaks with specific spatial frequencies in units cycles/pixel (Section 8.6). The horizontal and vertical profiles (Section 8.7) give a quick direct view of all possible types of nonuniformities. Finally, the characterization of defect pixels by logarithmically scaled histograms (Sections 4.4 and 8.8) is a flexible method to specify unusable or defect pixels according to application specific criteria.

4.2 Spatial Variances

Spatial variances can be computed from just two images taken at the same exposure as the variance of the temporal noise (Section 2.5). Subtracting the terms in Eqs. (17) and (18) yields

$$\begin{aligned} s_y^2 &= \frac{1}{NM}\sum_{m=0}^{M-1}\sum_{n=0}^{N-1}(y[0][m][n]-\mu[0])(y[1][m][n]-\mu[1]) \\ &= \frac{1}{NM}\left(\sum_{m=0}^{M-1}\sum_{n=0}^{N-1}y[0][m][n]y[1][m][n]\right)-\mu[0]\mu[1] \end{aligned} \tag{32}$$

It has been shown theoretically [18] that this expression never becomes negative. This can only happen if the correction for the difference in the two mean values in Eq. (18) would not be applied.

空域不一致性的评价方法

For all other evaluation methods of spatial nonuniformities besides variances, such as histograms, profiles, and spectrograms, it is required to suppress the temporal noise well below the spatial variations. This can only be performed by averaging over a sufficiently large number L of images. In this case, spatial variances are computed in the following way. First a mean image averaged over L images $\boldsymbol{y}[l]$ is computed:

$$\langle \boldsymbol{y} \rangle = \frac{1}{L} \sum_{l=0}^{L-1} \boldsymbol{y}[l]. \tag{33}$$

The averaging is performed over all pixels of a sensor array. The mean value of this image is given by:

$$\mu_y = \frac{1}{MN} \sum_{m=0}^{M-1} \sum_{n=0}^{N-1} \langle y \rangle [m][n], \tag{34}$$

where M and N are the number of rows and columns of the image and m and n the row and column indices of the array, respectively. Likewise, the *spatial variance* s^2 is

$$s^2_{y.\text{measured}} = \frac{1}{MN} \sum_{m=0}^{M-1} \sum_{n=0}^{N-1} (\langle y \rangle [m][n] - \mu_y)^2. \tag{35}$$

All spatial variances are denoted with the symbol s^2 to distinguish them easily from the temporal variances σ^2. The spatial variances computed from L averaged images have to be corrected for the residual variance of the temporal noise. This is why it is required to subtract σ_y^2/L:

$$s^2_{y.\text{stack}} = s^2_{y.\text{measured}} - \sigma_y^2/L. \tag{36}$$

4.3 Column, Row, and Pixel Spatial Variances

Modern CMOS sensors may exhibit not only pixel-to-pixel nonuniformities, but also row-to-row and/or column-to-column nonuniformities. This means that it is important to decompose the spatial variance into row, column, and pixel variances:

$$s_y^2 = s^2_{y.\text{row}} + s^2_{y.\text{col}} + s^2_{y.\text{pixel}}. \tag{37}$$

This decomposition applies also for line-scan cameras with a slightly different meaning. Because in the end any line-scan camera acquires images, row variations are caused by temporal variations from row to row.

With the proposed split of the spatial variances, there are now three unknowns instead of only one unknown. All three unknowns can still be estimated by computing additional spatial variances from a row and column averaged over the whole image.

The variances can be computed for each exposure step from only two images or for a more detailed analysis from an average over many images. Therefore the following equations are written in a general way using a mean image $\langle \boldsymbol{y} \rangle$ according to Eq. (33) averaged over L images. The mean row, mean column, and mean value are then given by

$$\mu_y[n] = \frac{1}{M} \sum_{m=0}^{M-1} \langle y \rangle [m][n], \quad \mu_y[m] = \frac{1}{N} \sum_{n=0}^{N-1} \langle y \rangle [m][n], \quad \mu_y = \frac{1}{MN} \sum_{m=0}^{M-1} \sum_{n=0}^{N-1} \langle y \rangle [m][n]. \tag{38}$$

The *column spatial variance* computed from the average row

$$s^2_{y.\text{col}} = \frac{1}{N} \sum_{n=0}^{N-1} (\mu_y[n] - \mu_y)^2 - s^2_{y.\text{pixel}}/M - \sigma_y^2/(LM) \tag{39}$$

still contains a residual *pixel spatial variance* and temporal variance, because the averaging over M rows does not completely suppress theses variances. Therefore the two terms on the right hand need to be subtracted.

Likewise, the *row spatial variance* computed from the average column

$$s^2_{y.\mathrm{row}} = \frac{1}{M}\sum_{m=0}^{M-1}(\mu_y[m]-\mu_y)^2 - s^2_{y.\mathrm{pixel}}/N - \sigma^2_y/(LN) \tag{40}$$

contains residual *pixel spatial variance* and temporal variance from averaging over N columns, and these also need to be subtracted.

The three equations (37), (39), and (40) form a linear equation system from which all three components of the spatial variance can be computed. With the two abbreviations

$$\begin{aligned} s^2_{y.\mathrm{cav}} &= \frac{1}{N}\sum_{n=0}^{N-1}(\mu_y[n]-\mu_y)^2 \quad - \quad \sigma^2_y/(LM), \\ s^2_{y.\mathrm{rav}} &= \frac{1}{M}\sum_{m=0}^{M-1}(\mu_y[m]-\mu_y)^2 \quad - \quad \sigma^2_y/(LN), \end{aligned} \tag{41}$$

the linear equation system reduces to

$$\begin{bmatrix} 1 & 0 & 1/M \\ 0 & 1 & 1/N \\ 1 & 1 & 1 \end{bmatrix} \begin{bmatrix} s^2_{y.\mathrm{col}} \\ s^2_{y.\mathrm{row}} \\ s^2_{y.\mathrm{pixel}} \end{bmatrix} = \begin{bmatrix} s^2_{y.\mathrm{cav}} \\ s^2_{y.\mathrm{rav}} \\ s^2_y \end{bmatrix}. \tag{42}$$

Solving this linear equation system yields

$$\begin{bmatrix} s^2_{y.\mathrm{col}} \\ s^2_{y.\mathrm{row}} \\ s^2_{y.\mathrm{pixel}} \end{bmatrix} = \frac{1}{MN-M-N} \begin{bmatrix} M(N-1) & N & -N \\ M & N(M-1) & -M \\ -MN & -NM & NM \end{bmatrix} \begin{bmatrix} s^2_{y.\mathrm{cav}} \\ s^2_{y.\mathrm{rav}} \\ s^2_y \end{bmatrix} \tag{43}$$

or

$$\begin{aligned} s^2_{y.\mathrm{col}} &= \frac{MN-M}{MN-M-N}s^2_{y.\mathrm{cav}} - \frac{N}{MN-M-N}(s^2_y - s^2_{y.\mathrm{rav}}), \\ s^2_{y.\mathrm{row}} &= \frac{MN-N}{MN-M-N}s^2_{y.\mathrm{rav}} - \frac{M}{MN-M-N}(s^2_y - s^2_{y.\mathrm{cav}}), \\ s^2_{y.\mathrm{pixel}} &= \frac{MN}{MN-M-N}(s^2_y - s^2_{y.\mathrm{cav}} - s^2_{y.\mathrm{rav}}) \end{aligned} \tag{44}$$

For large M and N, the solution simplifies to

$$\begin{aligned} s^2_{y.\mathrm{col}} &\approx s^2_{y.\mathrm{cav}}, \\ s^2_{y.\mathrm{row}} &\approx s^2_{y.\mathrm{rav}}, \\ s^2_{y.\mathrm{pixel}} &\approx s^2_y - s^2_{y.\mathrm{cav}} - s^2_{y.\mathrm{rav}} \end{aligned} \tag{45}$$

This approximative solution is only given for easier understanding, the computations should be performed with the exact solution Eq. (44).

4.4 Defect Pixels

As application requirements differ, it will not be possible to find a common denominator to exactly define when a pixel is defective and when it is not. Therefore it is more appropriate to provide *statistical information* about pixel properties in the form of histograms. In this way anybody can specify how many pixels are unusable or defective using application-specific criteria.

4.4.1 Logarithmic Histograms It is useful to plot the histograms with logarithmic y-axis for two reasons (Fig. 2a). Firstly, it is easy to compare the measured histograms with a normal distribution, which shows up as a negatively shaped parabola in a logarithmic plot. Thus it is easy to see deviations from normal distributions. Secondly, even single outliers can be distinguished from the many pixels following the normal distribution.

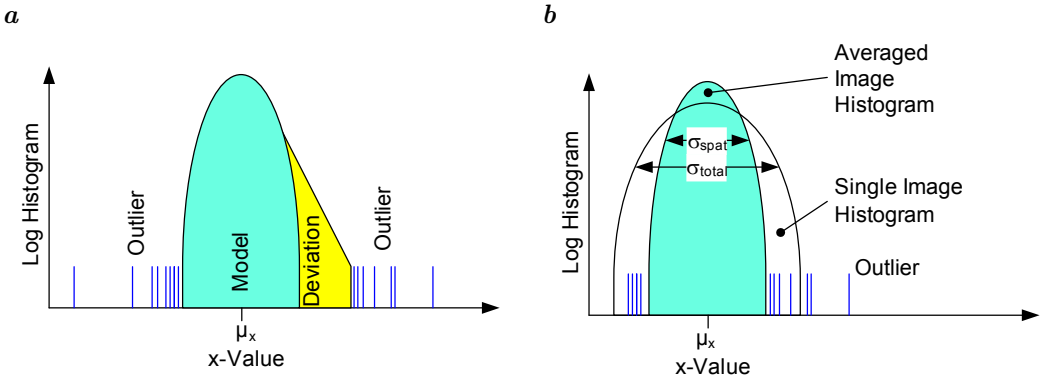

Figure 2: *Logarithmic histogram of spatial variations* ***a*** *Showing comparison of data to model and identification of deviations from the model and of outliers,* ***b*** *Comparison of logarithmic histograms from single images and averaged over many images.*

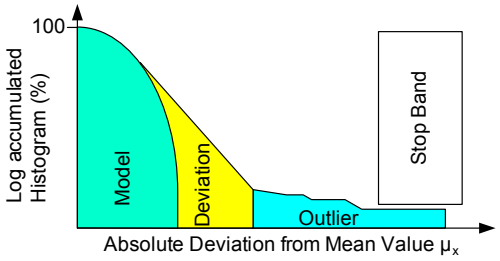

Figure 3: *Accumulated histogram with logarithmic y-axis.*

All histograms have to be computed from pixel values that come from averaging over many images. In this way the histograms only reflect the statistics of the spatial noise and the temporal noise is averaged out. The statistics from a single image is different. It contains the total noise, i.e. the spatial and the temporal noise.

It is hard to generally predict how far a deviation from the model will impact the final applications. Some of them will have human spectators, while others use a variety of algorithms to make use of the images. While a human spectator is usually able to work well with pictures in which some pixels show odd behaviors, some algorithms may suffer from it. Some applications will require defect-free images, some will tolerate some outliers, while others still have problems with a large number of pixels slightly deviating. All this information can be read out of the logarithmic histograms.

4.4.2 Accumulated Histograms A second type of histogram, the accumulated histogram is useful in addition (Fig. 3). It is computed to determine the ratio of pixels deviating by more than a certain amount. This can easily be connected to the application requirements. Quality criteria from camera or chip manufacturers can easily be drawn in this graph. Usually the criteria is, that only a certain amount of pixels deviates more than a certain threshold. This can be reflected by a rectangular area in the graph. Here it is called *stop band* in analogy to drawings from high-frequency technologies that should be very familiar to electronics engineers.

Table 1: *List of all EMVA 1288 measurements with classification into mandatory and optional measurements.*

Type of measurement	Mandatory	Reference
Sensitivity, temporal noise and linearity	Y	Section 6
Nonuniformity	Y	Sections 8.2 and 8.6
Defect pixel characterization	Y	Section 8.8
Dark current	Y	Section 7.1
Temperature dependence on dark current	N	Section 7.2
Spectral measurements $\eta(\lambda)$	N	Section 9

5 Overview Measurement Setup and Methods

The characterization according to the EMVA 1288 standard requires three different measuring setups:

1. A setup for the measurement of sensitivity, linearity and nonuniformity using a homogeneous monochromatic light source (Sections 6 and 8).
2. The measurement of the temperature dependency of the dark current requires some means to control the temperature of the camera. The measurement of the dark current at the standard temperature requires no special setup (Section 7).
3. A setup for spectral measurements of the quantum efficiency over the whole range of wavelengths to which the sensor is sensitive (Section 9).

Each of the following sections describes the measuring setup and details the measuring procedures. All camera settings (besides the variation of exposure time where stated) *must be identical* for all measurements. For different settings (e. g., gain) different sets of measurements must be acquired and different sets of parameters, containing all parameters which may influence the characteristic of the camera, must be presented. Line-scan sensors are treated as if they were area-scan sensors. Acquire at least 100 lines into one image and then proceed as with area-scan cameras for all evaluations except for the computation of vertical spectrograms (Section 8.6).

Not all measurements are mandatory as summarized in Table 1. A data sheet is only EMVA 1288 compliant if the results of *all* mandatory measurements from at least one camera are reported. If optional measurements are reported, these measurements must fully comply to the corresponding EMVA 1288 procedures.

All example evaluations shown in Figs. 5–16 come from simulated data — and thus served also to verify the methods and algorithms. A 12-bit 640×480 camera was simulated with a quantum efficiency $\eta = 0.5$, a dark value of 29.4 DN, a gain $K = 0.1$, a dark noise $\sigma_d = 30\,\mathrm{e}^-$ ($\sigma_{y.\mathrm{dark}} = 3.0$ DN), and with slightly nonlinear camera characteristics. The DSNU has a white spatial standard deviation $s_w = 1.5$ DN and two sinusoidal patterns with an amplitude of 1.5 DN and frequencies in horizontal and vertical direction of 0.04 and 0.2 cylces/pixel, respectively. The PRNU has a white spatial standard deviation of 0.5%. In addition, a slightly inhomogenous illumination with a quadratic fall-off towards the edges by about 3% was simulated.

6 Methods for Sensitivity, Linearity, and Noise

6.1 Geometry of Homogeneous Light Source

For the measurement of the sensitivity, linearity and nonuniformity, a setup with a light source is required that irradiates the image sensor homogeneously without a mounted lens. Thus the sensor is illuminated by a diffuse disk-shaped light source with a diameter D placed in front of the camera (Fig. 4a) at a distance d from the sensor plane. Each pixel must receive light from the whole disk under an angle. This can be defined by the *f-number*

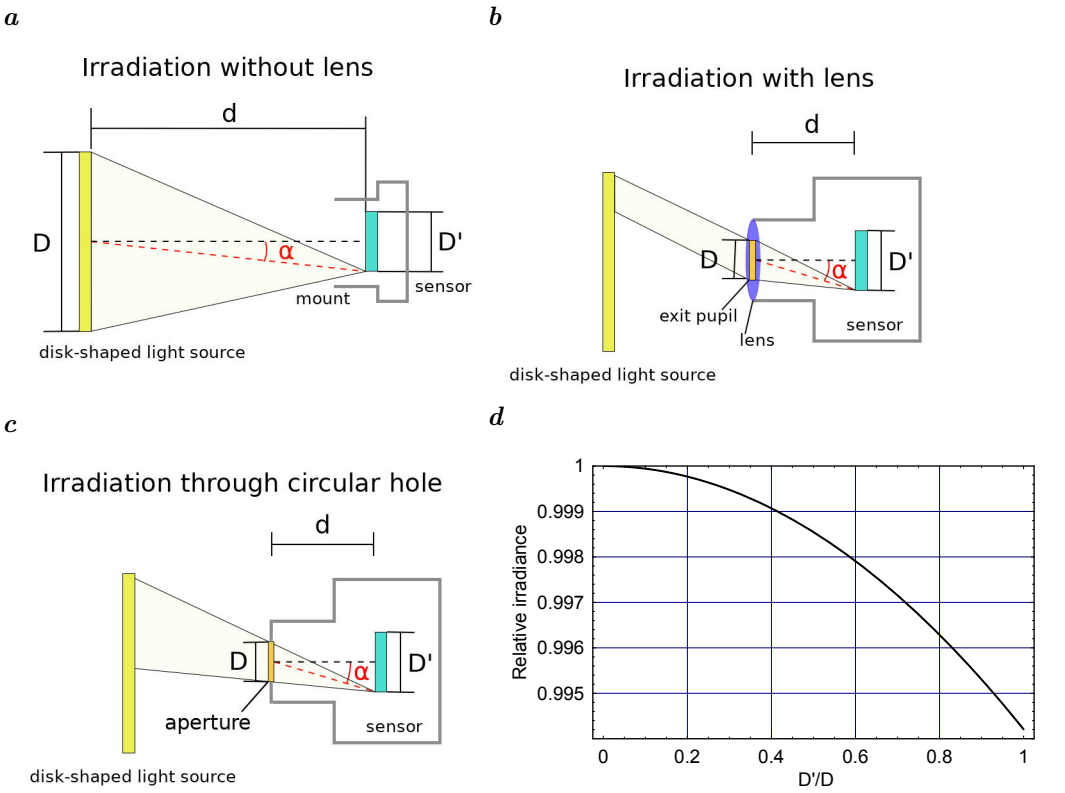

Figure 4: *Optical setup for the irradiation of the image sensor* **a** *without a lens,* **b** *with a lens, and* **c** *through a circular hole by a disk-shaped light source. The dashed red line is the chief ray at the edge of the sensor with an angle α to the optical axis, also denoted as the chief ray angle (CRA).* **d** *Relative irradiance at the edge of a image sensor with a diameter D', illuminated by a perfect integrating sphere with an opening D at a distance $d = 8D$.*

of the setup, which is is defined as:

$$f_{\#} = \frac{d}{D}. \tag{46}$$

Measurements performed according to the standard require an f-number of 8.

The best available homogeneous light source is an integrating sphere. Therefore it is not required but recommended to use such a light source. But even with a perfect integrating sphere, the homogeneity of the irradiation over the sensor area depends on the diameter of the sensor, D' [19, 20]. For a distance $d = 8 \cdot D$ (f-number 8) and a diameter D' of the image sensor equal to the diameter of the light source, the decrease is only about 0.5% (Fig. 4d). Therefore the diameter of the sensor area should not be larger than the diameter of the opening of the light source.

A real illumination setup even with an integrating sphere has a much worse inhomogeneity, due to one or more of the following reasons:

Reflections at lens mount. Reflections at the walls of the lens mount can cause significant inhomogeneities, especially if the inner walls of the lens mount are not suitably designed and are not carefully blackened and if the image sensor diameter is close to the free inner diameter of the lens mount.

Anisotropic light source. Depending on the design, a real integrating sphere will show some residual inhomogeneities. This is even more the case for other types of light sources.

Therefore it is essential to specify the spatial nonuniformity of the illumination, ΔE. It should be given as the difference between the maximum and minimum irradiance over the area of the measured image sensor divided by the average irradiance in percent:

$$\Delta E[\%] = \frac{E_{\max} - E_{\min}}{\mu_E} \cdot 100. \tag{47}$$

It is recommended that ΔE is not larger than 3%. This recommendation results from the fact that the linearity should be measured over a range from 5–95% of the full range of the sensor (see Section 6.9).

A weak point in the definition of the irradiation geometry of a sensor is that it only specifies the f-number, but not the position of the exit pupil, here simply the distance d to the spherical opening of the light source. For typical EMVA 1288 measuring equipment, the position of the light source is much further away than the exit pupil of lenses. The irradiation conditions are almost as for image-sided telecentric lenses. This can also cause vignetting, for instance, if a full-format image sensor with a 42 mm image circle is used with an F-mount camera. Because of the condition that the diameter D' of the image sensor must be smaller than the diameter D of the light source, the angle α of the chief ray at the edge of the sensor (Fig. 4a) is $\alpha < \arctan(d/2D) \approx 3.6^{\circ}$.

EMVA 1288 measurements will not give useful results if a sensor has microlenses, whose center is shifted away from the center of a pixel towards the edge of the sensor to adapt to the oblique chief ray angle of a lens with short exit pupil distance to the sensor. In this case the irradiation condition described above, will result in a significant fall-off of the signal towards the edge of the sensor.

Therefore with Release 4, optional EMVA 1288 measurements can also be done with camera lens combinations. For a standard measurement, the lens f-number must be set to 8 and focused to infinity. The calibration must also be performed with the lens (for details see Section 6.4). In this case, the camera lens combination looks into a light source (Fig. 4b) which must be homogeneous and isotropic for the whole field angle of the lens. All EMVA 1288 measurements can be performed in this way. It is important to note that the measured PRNU now includes the combined effect of lens and sensor. However, this is very useful to investigate, which camera/lens combination results in the lowest possible fall-off towards the edge. In order to be independent of a specific lens and mimic only the geometry of the irradiation, instead of a lens a circular hole with the exit pupil distance d corresponding to the design chief ray angle (α or CRA) of the image sensor can be used (Fig. 4c). The exit pupil distance d and the diameter of the aperture D are related to the CRA of an image sensor with a diameter D' by

$$d = \frac{D'/2}{\tan\alpha} \quad \text{and} \quad D = \frac{d}{f_{\#}}. \tag{48}$$

Of course, additional optional measurements can be performed with other f-numbers or a lens focused to a given working distance if this is of importance for a given application. Of special interest are measurements with lower f-numbers, in order to examine to what extent the wide cone of a fast lens is captured by the image sensor.

6.2 Spectral and Polarization Properties of Light Source

The guiding principle for all types of sensors is the same: Choose the type of irradiation that gives the maximum response. In other words, that type for which the corresponding camera channel was designed for. In order to compute the mean number of photons hitting the pixel during the exposure time (μ_p) from the image irradiance E at the sensor plane according to Eq. (4), narrow-band irradiation must be used in all cases. Only then is it possible to perform the measurements without the need to know the spectral response of the camera, which is only an optional measurement (Table 1).

For *gray-scale cameras* it is therefore recommended to use a light source with a center wavelength matching the maximum quantum efficiency of the camera under test. As required by the application, additional measurements with any other wavelength can always be performed. The *full width half maximum* (FWHM) of the light source should be less than 50 nm.

For the measurement of *color cameras* or *multispectral cameras*, the light source must be operated with different wavelength ranges, each wavelength range must be close to the maximum response of one of the corresponding color channels. Normally these are the colors blue, green, and red, but it could be any combination of color channels including channels in the ultraviolet and infrared. For color cameras and multispectral cameras the FWHM should be smaller than the bandwidth of the corresponding channel.

Such light sources can be achieved, e. g., by a light emitting diode (LED) or a broadband light source such as an incandescent lamp or an arc lamp with appropriate bandpass filters. The centroid wavelength λ_c, and the full width half maximum (FWHM) of the light source must be specified. The centroid wavelength of the light source is used for computation of the number of photons according to Eq. (3).

The best approach is to measure these quantities directly using a spectrometer. It is also valid to use the specifications given from the manufacturer of the light source. For a halogen light source with a bandpass filter, a good estimate of the spectral distribution of the light source is given by multiplying the corresponding blackbody curve with the transmission curve of the filter.

The measurement of *polarization cameras* requires light with *linear polarization*. The requirements for the *degree of linear polarization* P (Section 2.2) are high. The quantity $1 - P$ should be at least ten times lower than the expected value for the polarizing image sensor. The polarization angle of the light is aligned with the first polarization channel by searching the maximum average response from this channel. For measurements of residual polarization effects with normal cameras, this step is not required.

6.3 Variation of Irradiation

Basically, there are three possibilities to vary the radiant exposure of the sensor, i. e., the radiation energy per area received by the image sensor:

I. Constant illumination with variable exposure time.
With this method, the light source is operated with constant radiance and the radiant exposure is changed by the variation of the exposure time. The radiant exposure H is given as the irradiance E times the exposure time t_{exp} of the camera. Because the dark signal generally may depend on the exposure time, it is required to measure the dark image at *every* exposure time used. The absolute calibration depends on the true exposure time being equal to the exposure time set in the camera.

II. Variable continuous illumination with constant exposure time.
With this method, the radiance of the light source is varied by any technically possible way that is sufficiently reproducible. With LEDs this is simply achieved by changing the current. The radiant exposure H is given as the irradiance E times the exposure time t_{exp} of the camera. Therefore the absolute calibration depends on the true exposure time being equal to the exposure time set in the camera.

III. Pulsed illumination with constant exposure time.
With this method, the radiant exposure of the sensor is varied by the pulse length of the LED. When switched on, a constant current is applied to the LEDs. The radiant exposure H is given as the LED irradiance E times the pulse length t. The sensor exposure time is set to a constant value, which is larger than the maximum pulse length for the LEDs. The LEDs pulses are triggered by the "integrate enable" or "strobe out" signal from the camera. The LED pulse must have a short delay to the start of the integration time and it must be made sure that the pulse fits into the exposure interval so that there are no problems with trigger jittering. The pulsed illumination technique must not be used with rolling shutter mode. Alternatively it is possible to use an external trigger source in order to trigger the sensor exposure and the LED flashes synchronously.

According to basic assumptions number one and two made in Section 1.2, all three methods are equivalent because the amount of photons collected and thus the digital gray value depends only on the product of the irradiance $E(t)$ integrated over the exposure time. Depending on the available equipment and the properties of the camera to be measured, one of the three techniques for irradiation variation or a combination of them can be chosen.

6.4 Calibration of Irradiation

The irradiance must be calibrated absolutely by using a calibrated photodiode put at the place of the image sensor. The calibration accuracy of the photodiode as given by the calibration agency plus possible additional errors related to the measuring setup must be specified together with the data. The accuracy of absolute calibrations are typically between

3% and 5%, depending on the wavelength of the light. The reference photodiode should be recalibrated at least every second year. This will then also be the *minimum systematic error* of the measured quantum efficiency and all related parameters which contain photons in its units.

The radiant exposure H of a pixel with the total area A recieved during the exposure time t_{exp} in units of photons is computed according to Eq. (4). If pixel *binning* is applied, the area of a pixel has to be multiplied by the horzontal and vertical binning factor. Likewise for a *time delay integration* (TDI) sensor, where multiple exposures are accumulated, the exposure time is multiplied by the TDI factor.

For measurements with lens/camera combinations, the same calibration procedures can be applied. Because of the often significant lens shading, it is important that the photodiode is sufficiently small compared to the diameter of the image sensor for a correct calibration in the center of the sensor. A smaller diameter of a photodiode can easily be achieved by placing a pinhole in front of the photodiode. This pinhole must precisely be located in the same distance as the image sensor.

The precision of the calibration of the different irradiance levels must be much higher than the absolute accuracy in order to apply the photon transfer method (Sections 2.4 and 6.6) and to measure the linearity (Sections 2.1 and 6.9) of the sensor with sufficient accuracy. Therefore, the standard deviation of the calibration curve from a linear regression must be lower than 0.1% of the maximum value.

6.5 Measurement Conditions for Linearity and Sensitivity

Temperature. The measurements are performed at room temperature or a controlled temperature elevated above the room temperature. The type of temperature control must be specified. Measure the temperature of the camera housing by placing a temperature sensor at the lens mount with good thermal contact. If a cooled camera is used, specify the set temperature. Do not start measurements before the camera has come into thermal equilibrium.

Digital resolution. Set the number of bits as high as possible in order to minimize the effects of quantization on the measurements.

Gain. Set the gain of the camera as small as possible without saturating the signal due to the full well capacity of any pixel (this almost never happens). If with this minimal gain, the dark noise $\sigma_{y.\text{dark}}$ is smaller than 0.5 DN, the dark noise cannot be measured reliably. (This happens only in the rare case of a 8-bit camera with a high-quality sensor.) Then only an upper limit for the temporal dark noise can be calculated. The dynamic range is then limited by the quantization noise.

Offset. Set the offset of the camera as small as possible but large enough to ensure that the dark signal including the temporal noise and spatial nonuniformity does not cause any significant underflow. This can be achieved by setting the offset at a digital value so that less than about 0.5% of the pixels underflow, i. e., have the value zero. This limit can easily be checked by computing a histogram and ensures that not more than 0.5% of the pixels are in the bin zero.

Distribution of radiant exposure values. Use at least 50 about equally spaced radiant exposures resulting in digital gray value from the dark gray value and the maximum digital gray value. Only for production measurements as few as 9 suitably chosen values can be taken.

Number of measurements taken. Capture two images at each exposure level. To avoid transient phenomena when the live grab is started, the two images are taken from a live image series. It is also required to capture two images each without exposure (dark images) at *each* exposure time used for a proper determination of the mean and variance of the dark gray value, which may depend on the exposure time (Section 3).

6.6 Evaluation of the Measurements According to the Photon Transfer Method

As described in Section 2, the application of the photon transfer method and the computation of the quantum efficiency requires the measurement of the mean gray values and the temporal

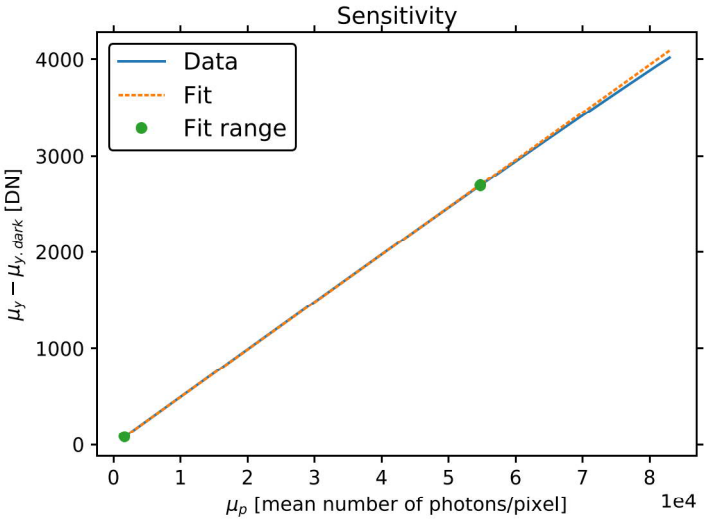

Figure 5: *Example of the characteristic curve to determine the responsivity $R = K\eta$ of a camera. The graph draws the measured mean photo-induced gray values $\mu_y - \mu_{y.dark}$ versus the radiant exposure μ_p in units photons/pixel and the linear regression line used to determine $R = K\eta$. The red dots marks the 0 – 70% range of saturation that is used for the linear regression. For multichannel cameras, the graph must contain these items for all channels.*

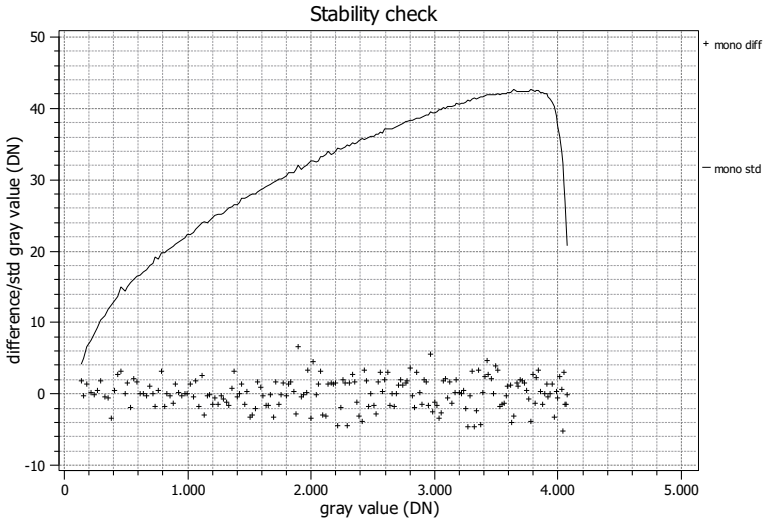

Figure 6: *Example of a stability graph. The graph shows the temporal standard deviation according to Eq. (18) and the difference of the mean of the two consecutively captured images, $\mu[0] - \mu[1]$, versus the mean photo-induced gray values $\mu_y - \mu_{y.dark}$.*

variance of the gray together with the irradiance per pixel in units photons/pixel. The method to compute the mean and variance are given in Section 2.5.

The measured mean photo-induced gray values $\mu_y - \mu_{y.\mathrm{dark}}$ is shown versus the quantum exposure H in units photons/pixel in the *characteristic curve* (Fig. 5). If the exposure is changed by changing the exposure time (method I in Section 6.3), a second graph must be provided which shows $\mu_{y.\mathrm{dark}}$ as a function of the exposure time t_{exp}.

The temporal standard deviation σ_y according to Eq. (18) and the difference of the mean of the two consecutively captured images, $\mu[0] - \mu[1]$, versus the mean photo-induced gray values $\mu_y - \mu_{y.\mathrm{dark}}$ are shown in the *stability graph* Fig. 6.

The estimation of derived quantities according to the photon transfer method is per-

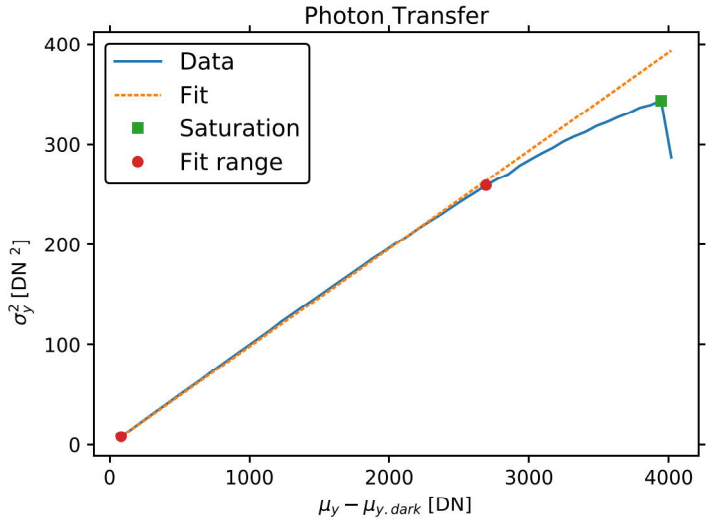

Figure 7: *Example of a photon transfer curve to determine the overall system gain K of a camera (photo transfer curve). The graph draws the measured variance σ_y^2 versus the mean photo-induced gray values $\mu_y - \mu_{y.dark}$ and the linear regression line used to determine the overall system gain K. The green dots mark the 0 – 70% range of saturation that is used for the linear regression. The system gain K is given with its one-sigma statistical uncertainty in percent, computed from the linear regression.*

formed as follows:

Saturation. The saturation gray value $\mu_{y.\mathrm{sat}}$ is given as the mean gray value where the histogram of the gray value distribution is not significantly cut-off so that the estimate of the mean value and especially the variance is not biased. With this technique it is required to first find the maximum possible value. For a sensor with a resolution of k bits, this is normally the value $2^k - 1$. But for some sensors, this may be a smaller value. Therefore it is first required to find the maximum possible value y. Then set the exposure by adjusting the exposure time and/or radiance of the light source just as high that between 0.1 - 0.2% of the total number of pixels show the maximum value. With this setting, the bias in the variance estimation is less than 0.37% for a normal distribution. Accumulate the histogram from one or two images without any averaging.

Responsivity R. According to Eq. (6), the slope of the relation

$$\mu_y - \mu_{y.\mathrm{dark}} = R\mu_p \quad \textit{Characteristic curve} \tag{49}$$

(with fixed zero offset) gives the responsivity $R = K\eta$. For this regression all data points must be used in the range between the minimum value and 70% saturation ($0.7 \cdot (\mu_{y.\mathrm{sat}} - \mu_{y.\mathrm{dark}})$) (Fig. 5).

Overall system gain K. According to Eq. (15), the slope of the relation

$$\sigma_y^2 = \sigma_{y.\mathrm{dark}}^2 + K(\mu_y - \mu_{y.\mathrm{dark}}) \quad \textit{Photon transfer curve} \tag{50}$$

gives the absolute gain factor K. Select the same range of data points as for the estimation of the responsivity (see above, and Fig. 7). Compute a least-squares linear regression of $\sigma_y^2 - \sigma_{y.\mathrm{dark}}^2$ versus μ_y over a saturation range from 0 to 70% with unknown offset and slope. Then the estimated slope is the gain factor K.

好准啊 之前测的线性区
正好在25/36
x100%=69.4444%

The estimated gain K is only correct if the the photon transfer curve is sufficiently linear. In order to check this apply the cubic B-spline regression introduced with this general model (see this document) to the photon transfer curve and compute at all n measurement points within the 0 to 70% saturation range the derivative of this spline regression function (local slope K_i). The mean of the magnitude of the relative deviations

must be smaller than 3%, i. e.,

cubic B-spline regression 因为不清楚怎么测mu_p，所以这个指标不清楚怎么测

$$\sum_{i=1}^{n} \frac{|K_i - K|}{K} < 0.03. \tag{51}$$

If this condition is met, the linear model can be used. Otherwise the evaluation of the measurements must be performed according to the general model.

Quantum efficiency η. The quantum efficiency η is given as the ratio of the responsivity $R = K\eta$ and the overall system gain K:

$$\eta = \frac{R}{K}. \tag{52}$$

For monochrome cameras, the quantum efficiency is thus obtained only for a single wavelength band with a bandwidth no wider than 50 nm. Because all measurements for color cameras are performed for all color channels, quantum efficiencies for all these wavelength bands are obtained and are to be reported. For color camera systems that use a color filter pattern any pixel position in the repeated pattern should be analyzed separately. For a Bayer pattern, for example, there are four color channels in total, mostly two separate green channels, a blue channel, and a red channel.

Temporal dark noise. Independent of the illumination method (Section 6.3), the temporal dark noise is measured at the lowest exposure of the camera in order to measure the lowest possible temporal dark noise. At higher exposure times, the temporal dark noise is higher (Section 7). Two values are reported.

1. The standard deviation of the temporal noise $\sigma_{y.\mathrm{dark}}$ in units of DN. This value gives the actual performance of the camera at the given bit resolution and includes the quantization noise.
2. In order to compute the temporal dark noise in units e^- (a quantity of the sensor *without* the effects of quantization), subtract quantization noise and use

$$\sigma_d = \sqrt{(\sigma^2_{y.\mathrm{dark}} - \sigma^2_q)} \Big/ K. \tag{53}$$

If $\sigma^2_{y.\mathrm{dark}} < 0.24$, the temporal noise is dominated by the quantization noise and no reliable estimate is possible (Section C.4). Then $\sigma_{y.\mathrm{dark}}$ must be set to 0.49 and the upper limit of the temporal dark noise in units e^- *without* the effects of quantization is given by

$$\sigma_d < \frac{0.40}{K}. \tag{54}$$

Absolute sensitivity threshold $\mu_{p.\mathrm{min}}$. Use definition Eq. (26) in Section 2.7 to compute the absolute sensitivity threshold $\mu_{p.\mathrm{min}}$.

Saturation capacity $\mu_{p.\mathrm{sat}}$. The saturation capacity $\mu_{p.\mathrm{sat}}$ is the number of photons which corresponds to the maximum measured digital value $\mu_{y.\mathrm{sat}}$ as described at the beginning of this section. The saturation capacity $\mu_{e.\mathrm{sat}}$ in e^- is given by Eq. (24).

Signal-to-noise ratio (SNR). The measured mean and the variance of the gray values are used to compute the SNR according to Eq. (20). These values are plotted in a double logarithmic plot together with the theoretical curve for the linear model Eq. (21) after using the measured quantum efficiency η and the temporal dark noise σ_d and the quantization noise (Fig. 8). Also compute the maximum achievable $\mathrm{SNR}_{\mathrm{max}}$ for the saturation exposure using

$$\mathrm{SNR}_{\mathrm{max}} = \sqrt{\mu_{e.\mathrm{sat}}} \tag{55}$$

and express this value as a ratio and in dB ($20 \log_{10}$ SNR).

Dynamic range (DR). Compute the dynamic range (Eq. (28) in Section 2.7) as the ratio of the saturation capacity $\mu_{p.\mathrm{sat}}$ (see beginning of this section) and the absolute sensitivity threshold $\mu_{p.\mathrm{min}}$ (Eq. (26)). It should be given as a ratio and in dB ($20 \log_{10}$ DR).

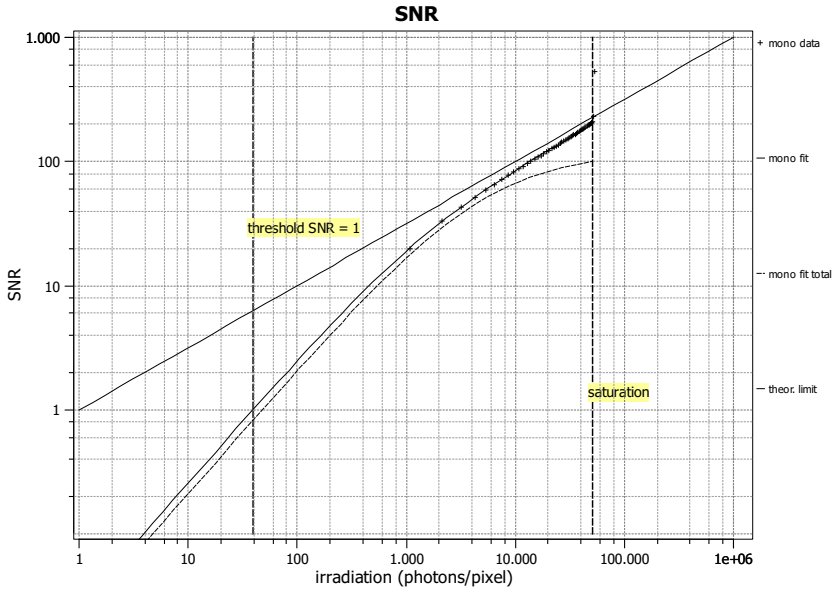

Figure 8: *Example of a SNR graph. It contains the measured SNR and SNR_{total} values, the theoretical curve according to the linear camera model Eq. (21) determined with the measured σ_d^2 and η values, the theoretical curve according to Eq. (69) including in addition the effect of spatial nonuniformities (DSNU and PRNU), and the SNR curve for an ideal sensor Eq. (23) with no dark and quantization noise and a quantum efficiency η of 1. The absolute sensitivity threshold and the saturation capacity are marked by vertical dashed lines.*

6.7 Evaluation of Multichannel Cameras

For any camera with multiple channels, each channel is evaluated separately. Thus all parameters in the previous section and following sections are computed for each channel with the same equations as for a monochrome camera. In this way it is not only possible to analyze color, multispectral and polarization cameras but also the raw channels of any type of multichannel cameras, provided the raw channel data can be accessed. One possible example are the multiple taps of a time-of-flight depth camera.

6.8 Evaluation of Derived Parameters 待研究

For derived quantities, the same methods can be applied to compute mean values and their temporal variance at all exposure steps as for raw data. Compute the derived parameters from the corresponding channels for all pixels from the two images taken at the same exposure *after* subtraction of an averaged dark image as it is used for a detailed analysis of nonuniformity, i. e., use $\boldsymbol{y}_j - \langle \boldsymbol{y}_{j.\mathrm{dark}} \rangle$ for all channels.

Care must only be taken in two cases:

- Parameters that are the ratio of two parameters as, e. g., for the degree of polarization (Section 2.3), cannot be computed in the dark, because the parameter is not defined in this case.
- *Circular parameters* such as the polarization angle for a polarization sensor or hue for a color sensor show a discontinuity from the maximum to the minimum value. In this case an indirect approach must be taken. Circular parameters show an equation of the following type, see Eq. (12):

$$\alpha = \arctan\left(\frac{y}{x}\right), \tag{56}$$

which can be used to compute the mean and variance of α using the laws of error propagation:

$$\mu_\alpha = \arctan\left(\frac{\mu_y}{\mu_x}\right), \quad \sigma_\alpha^2 = \frac{x^2\sigma_y^2 + y^2\sigma_x^2}{(x^2+y^2)^2}. \tag{57}$$

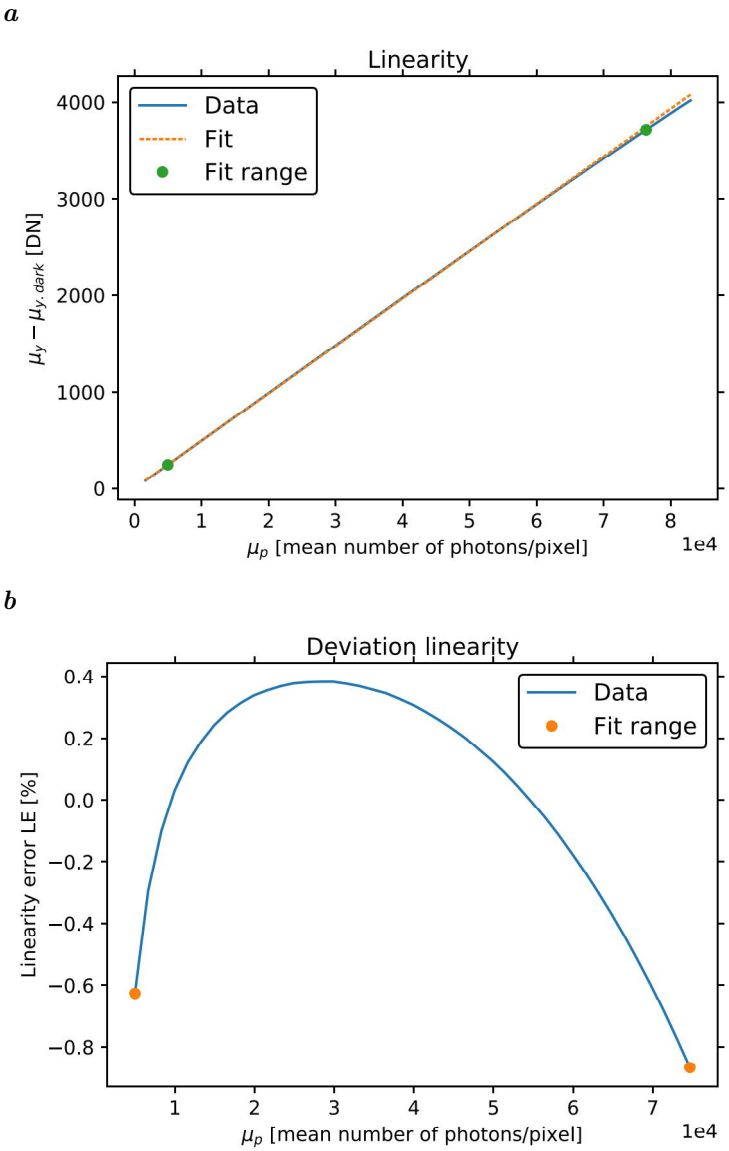

Figure 9: *Example for the evaluation of the linearity:* ***a*** *Mean gray value minus the dark value versus the quantum exposure plus the linear regression curve covering* all *measured values. The dots mark the 5 – 95% range of saturation that is used for the linearity regression.* ***b*** *Percentage of the deviation from the linear regression to determine the linearity error LE.*

Do not compute the mean of α over all pixels directly from the α values at all pixels, because close to the discontinuity erroneous results will be obtained. Instead it is required to compute the mean and variance from $\boldsymbol{x}$ and $\boldsymbol{y}$.

6.9 Evaluation of Linearity 算Linearity error

According to Section 6.5 at least 9 pairs of mean digital gray $\mu_y[i]$ and exposure values $H[i]$ are available. The linearity is determined by computing a least-squares linear regression minimizing the *relative* deviation in the digital gray value axis from the linear relation

$$y = a_0 + a_1 H \tag{58}$$

with an offset a_0 and a slope a_1 (Fig. 9a). In the following equations the abbreviation $y[i] = \mu_y[i] - \mu_{\text{y.dark}}[i]$ is used.[7] Because *relative* deviations are minimized, not

$$\sum_i \left[y[i] - (a_0 + a_1 H[i])\right]^2$$

is minimized but

$$\sum_i \frac{1}{y[i]^2} \left[y[i] - (a_0 + a_1 H[i])\right]^2 .$$

This is equivalent to a weighted least squares regression, where each data point $y[i]$ gets the weight $1/y[i]^2$. The resulting equations for estimating the offset a_0 and the slope a_1 are

$$a_0 = \frac{1}{\Delta}\left[\sum H[i]/y[i] \sum H[i]/y[i]^2 - \sum H[i]^2/y[i]^2 \sum 1/y[i]\right] \tag{59}$$

and

$$a_1 = \frac{1}{\Delta}\left[\sum H[i]/y[i]^2 \sum 1/y[i] - \sum H[i]/y[i] \sum 1/y[i]^2\right] \tag{60}$$

with

$$\Delta = \left(\sum H[i]/y[i]^2\right)^2 - \sum H[i]^2/y[i]^2 \sum 1/y[i]^2 \tag{61}$$

using the math for linear least squares regression [1, 21]. All sums in this section are computed with data values $y[i], H[i]$ in the range between 5% and 95% of the saturation capacity $\mu_{\text{y.sat}} - \mu_{\text{y.dark}}$.

Using this regression, the relative deviation from the regression can be computed by

$$\delta_y[i]\ [\%] = 100\,\frac{y[i] - (a_0 + a_1 H[i])}{a_0 + a_1 H[i]}. \tag{62}$$

The linearity error is then defined as the the mean of the absolute deviation in the range between 5% and 95% of the saturation capacity.

$$\text{LE} = \frac{1}{n}\sum_{i=1}^{n} |\delta_y[i]| \quad . \tag{63}$$

7 Methods for Dark Current

7.1 Evaluation of Dark Current at One Temperature

Dark current measurements require no illumination source. From Eqs. (29) and (30) in Section 3 it is evident that the dark current can either be measured from the linear increase of the mean or the variance of the dark gray value y_{dark} with the exposure time. The preferred method is, of course, the measurement of the mean, because the mean can be estimated more accurately than the variance. If, however, the camera features a dark current compensation, the dark current must be estimated using the variance.

At least six equally spaced exposure times must be chosen. It is recommended to choose much longer exposure times than for the sensitivity, linearity, and noise measurements, best to the maximum exposure time recommended by the camera manufacturer.

The dark current is then given as the slope in the relation between the exposure time and mean and variance of the dark value (Fig. 10). A linear least squares regression of the measured dark values gives the dark current in units DN/s and DN^2/s, respectively. Divide the values by the measured gain K and K^2, respectively, to obtain the dark current also in units e^-/s.

[7] The index i in $\mu_{\text{y.dark}}[i]$ applies only for method I to vary the exposure (see Section 6.3). For methods II and III it is a single mean dark value $\mu_{\text{y.dark}}$.

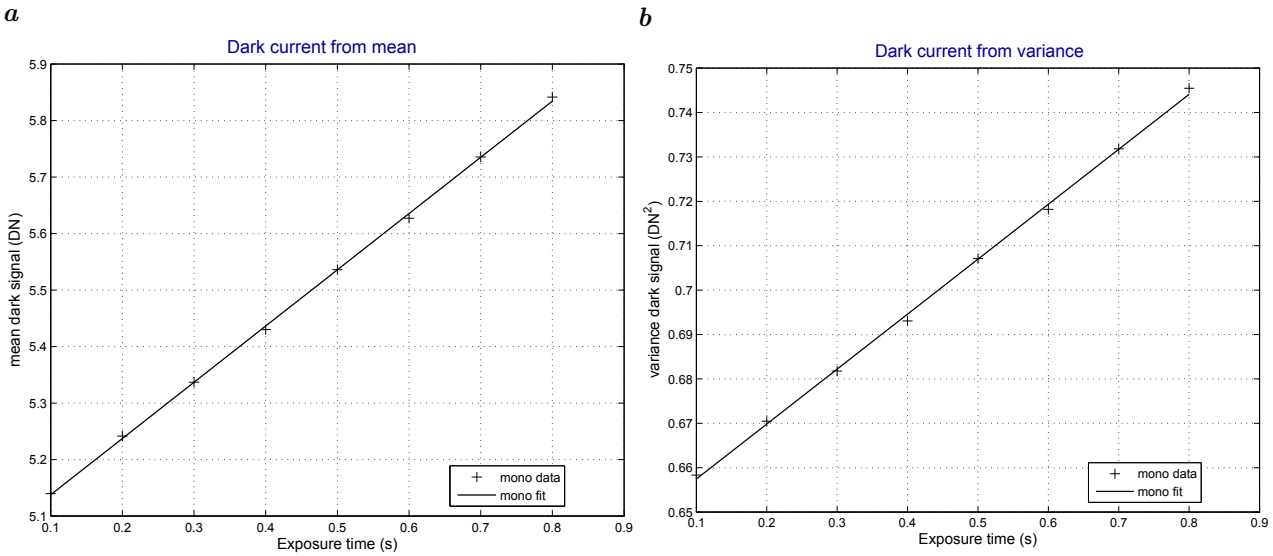

Figure 10: *Examples for dark current measurements: graph of the* **a** *dark value and* **b** *temporal variance versus the exposure time. The linear regressions line are also shown.*

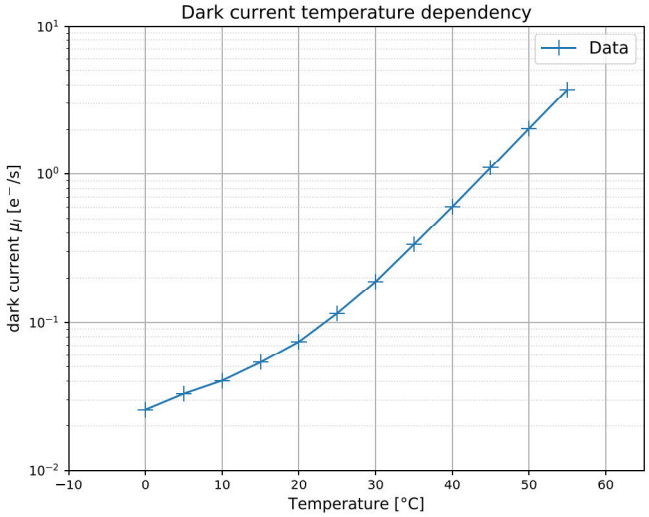

Figure 11: *Example of a measuring curve to determine the dark current temperature dependency. The graph draws the measured dark current μ_I in units e^-/s versus the temperature T.*

If the camera's exposure time is not set long enough to result in meaningful values for the dark current, this value still must be reported together with its one-sigma error from the regression. In this way at least an upper limit of the dark current can be given, provided that $\mu_I + \sigma_I > 0$.

The measured dark current can be used to estimate the standard deviation of the temporal noise at any exposure time t_{any}:

$$\sigma_{y.\text{dark}}(t_{\text{any}}) = \sqrt{\sigma^2_{y.\text{dark}}(t_{\text{exp}}) + \mu_{I.y}(t_{\text{any}} - t_{\text{exp}})} \tag{64}$$

and any other parameter derived from the temporal dark noise. The quantity t_{exp} is the exposure time at which the temporal dark noise was measured (Section 2.5).

7.2 Evaluation of Dark Current at Multiple Temperatures

The temperature dependency of the dark current is determined by measuring the dark current as described above for different housing temperatures. For temperatur measurement

see Section 6.5. The temperatures must vary over the whole range of the operating temperature of the camera and should include at least 6 equally spaced temperatures within this range. Put a capped camera in a climate exposure cabinet or control its temperature in another suitable way and drive the housing temperature to the desired value for the next measurement. For cameras with internal temperature regulation and cooling of the image sensor no climate cabinet is required. Then the temperature dependence of the dark current can only be measured in the temperature range that can be set.

After a temperature change wait until the camera values are stable. This is most easily done by continuously measuring the dark values at the largest exposure time. For each temperature, determine the dark current by taking a series of measurements with varying exposure times as described in Section 7.1.

The results of the temperature dependency of the dark current is reported in a dark current (logarithmic scale) versus temperature (linear scale) plot as shown in Fig. 11.

8 Methods for Spatial Nonuniformity and Defect Pixels

The measurements for spatial nonuniformity and the characterization of defect pixels are performed with the same setup as the sensitivity, linearity, and noise, described in Section 6. Therefore, the basic measuring conditions are also the same (Section 6.5).

All quantities describing nonuniformities, except for the spatial variances (Section 4.2), must be computed from mean gray values averaged over many images. This is because the variance of the temporal noise ($\sigma_y \approx 1\%$) is typically larger than or about the same as the variance of the spatial variations ($s_y \approx 0.3 - 1.0\%$). The temporal noise can only be suppressed by averaging over many images. Typically averaging over L =100–500 images is required. Because of the linear model, it is sufficient to apply the averaging over a sequence of dark images and a sequence of images at 50% saturation, resulting in $\langle \boldsymbol{y}_{\text{dark}} \rangle$ and $\langle \boldsymbol{y}_{50} \rangle$, respectively.

However, the variances introduced in Section 4.2, and only these, can be computed already with sufficient statistical certainty from only two images and are therefore available for each exposure step.

8.1 Correction for Uneven Illumination

This section addresses the problem that the photoresponse distribution may be dominated by gradual variations in illumination source, especially the typical fall-off of the irradiance towards the edges of the sensor. Low-frequency spatial variations of the image sensor, however, are of less importance, because of two reasons. Firstly, lenses introduce a fall-off towards the edges of an image (*lens shading*). Except for special low-shading lenses, this effect makes a significant contribution to the low-frequency spatial variations. Secondly, almost all image processing operations are not sensitive to gradual gray value changes. (See also discussion in Section 4.1 under item gradual variations.)

In order to show the properties of the camera rather than the properties of an imperfect illumination system, a highpass filter is applied before performing all nonuniformity related computations. In this way the effect of low spatial frequency sensor properties is suppressed. This includes all statistical parameters (Sections 4.2 and 8.3), spectrograms (Section 8.6), and all histograms for defect pixel characterization (Section 8.8). Only for the horizontal and vertical profiles (Section 8.7) no highpass filtering is applied. This means that the profiles show also the large scale nonuniformity but can be biased by an uneven illumination.

For highpass filtering the following two-step filtering is applied. First the images are smoothed by the following filters, one applied after the other: A 7×7 box filter, an 11×11 box filter, and a 3×3 binomial filter. In a second step this smoothed image is subtracted form the original image, leaving only the high-frequency part of the nonuniformities in the resulting image. Theoretical details for this choice of highpass filtering are detailed in Appendix E.3.

8.2 Spatial Standard Deviations

For a detailed analysis of spatial nonuniformity it is also required to compute spatial variances from the stack of L images according to the equations given in Section 4.2. The variance of the temporal noise must be computed directly from the same stack of images $\boldsymbol{y}[l]$ as the mean of the variance at every pixel using

$$\sigma^2_{s[m][n]} = \frac{1}{L-1}\sum_{l=0}^{L-1}\left(y[l][m][n] - \frac{1}{L}\sum_{l=0}^{L-1}y[l][m][n]\right)^2 \quad \text{and} \quad \sigma^2_{y.\text{stack}} = \frac{1}{MN}\sum_{m=0}^{M-1}\sum_{n=0}^{N-1}\sigma^2_{s[m][n]}. \tag{65}$$

8.3 DSNU, and PRNU

The DSNU_{1288} and PRNU_{1288} values are then given by

$$\text{DSNU}_{1288} = s_{y.\text{dark}}/K \qquad (\text{units e}^-) \tag{66}$$

and

$$\text{PRNU}_{1288} = \frac{\sqrt{s^2_{y.50} - s^2_{y.\text{dark}}}}{\mu_{y.50} - \mu_{y.\text{dark}}} \qquad (\text{units \%}). \tag{67}$$

from highpass-filtered images.

The index 1288 has been added to these definitions because many different definitions of these quantities can be found in the literature. The DSNU_{1288} is expressed in units e^-; by multiplying with the overall system gain K it can also be given in units DN. The PRNU_{1288} is defined as a standard deviation relative to the mean value. In this way, the PRNU_{1288} gives the spatial standard deviation of the photoresponse nonuniformity in % from the mean.

All the equations in this section are not only applied to the total spatial variance, but also to the column, row, and pixel variances. The corresponing DSNUs and PRNUs are denoted by $\text{DSNU}_{1288.\text{col}}$, $\text{DSNU}_{1288.\text{row}}$, $\text{DSNU}_{1288.\text{pixel}}$, $\text{PRNU}_{1288.\text{col}}$, $\text{PRNU}_{1288.\text{row}}$, and $\text{PRNU}_{1288.\text{pixel}}$.

8.4 Spatial Standard Deviations of Derived Parameters

In the same way as temporal standard deviations can be computed for parameters derived from more one or more channels (Section 6.8) it is also possible to compute standard deviations of spatial nonuniformities for these quantities.

8.5 Total SNR

The DSNU_{1288} and PRNU_{1288} values can be used to include the spatial nonuniformites into the SNR resulting in the total SNR. From the definition of the PRNU_{1288} in Eq. (67), the variance s^2_y can be expressed as

$$s^2_y = s^2_{y.\text{dark}} + (\text{PRNU}_{1288})^2 (\mu_y - \mu_{y.\text{dark}})^2$$

With the definition of DSNU_{1288} in Eq. (66) and substituting the mean values by the mean number of photons using the sensitivity curve Eq. (6) the variance of the spatial inhomogeneity in units DN^2 is given by

$$s^2_y = K^2\text{DSNU}^2_{1288} + \text{PRNU}^2_{1288}K^2 (\eta\mu_p)^2 . \tag{68}$$

The variance term s^2_y/K^2 (units e^-) due to the spatial nonuniformity can be added to the SNR to yield the total SNR:

$$\boxed{\text{SNR}_{\text{total}}(\mu_p) = \frac{\eta\mu_p}{\sqrt{\sigma^2_d + \text{DSNU}^2_{1288} + \sigma^2_q/K^2 + \eta\mu_p + \text{PRNU}^2_{1288}(\eta\mu_p)^2}}.} \tag{69}$$

This model curve and the measured values of the total SNR at all exposure steps has to be added to the SNR plot in Fig. 8.

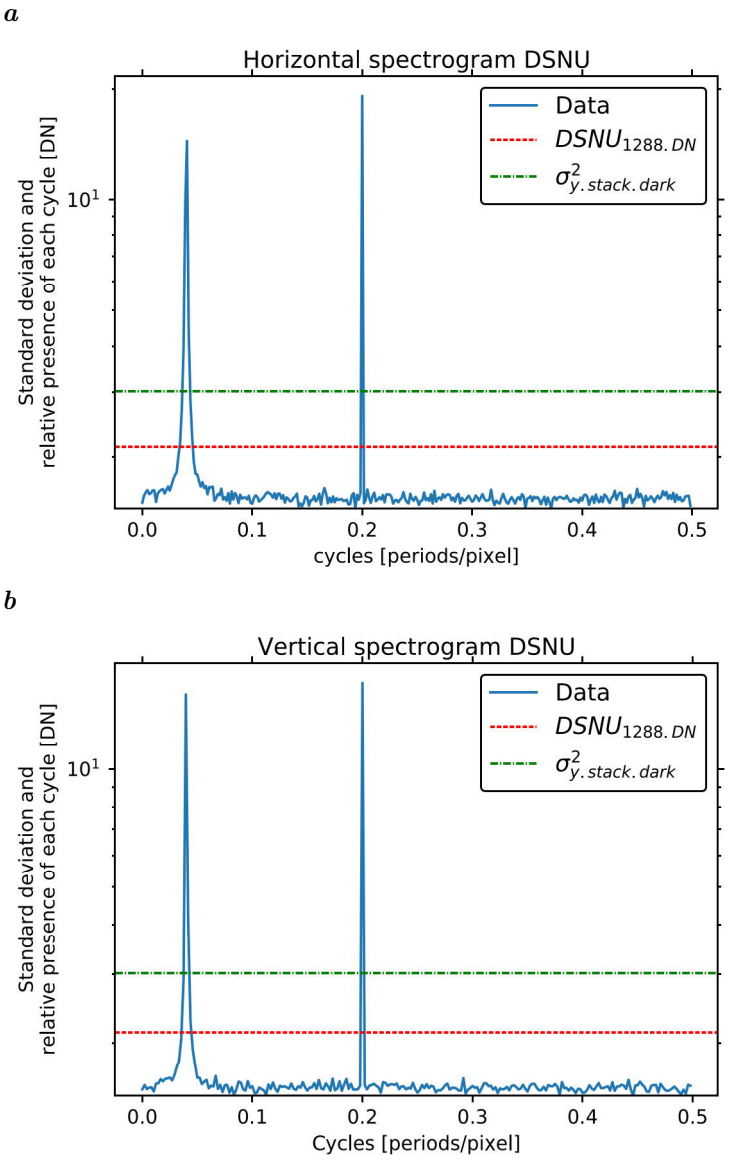

Figure 12: *Example for spectrograms of the dark image:* ***a*** *horizontal spectrogram,* ***b*** *vertical spectrogram, together with a two horizontal lines: One marks the white noise spectrum corresponding to the standard deviation of the dark temporal noise $\sigma_{y.stack.dark}$ for acquiring a single image without averaging and the second the DSNU. A comparison of the spectrogram with the DSNU reveals how much peaks in the spectrogram contribute to the DSNU.*

8.6 Horizontal and Vertical Spectrograms

Spectrograms are computed from the highpass-filtered DSNU image $\langle \boldsymbol{y}_{\text{dark}} \rangle$ and the PRNU image $\langle \boldsymbol{y}_{50} \rangle - \langle \boldsymbol{y}_{\text{dark}} \rangle$ (compare Section 8.1). Computation of a spectrogram from the 50% saturation image $\langle \boldsymbol{y}_{50} \rangle$ is optional. The computation of the horizontal spectrograms requires the following computing steps:

1. Subtract the mean value from the image $\boldsymbol{y}$.
2. Compute the Fourier transform of each row vector $\boldsymbol{y}[m]$:

$$\hat{y}[m][v] = \frac{1}{\sqrt{N}} \sum_{n=0}^{N-1} y[m][n] \exp\left(-\frac{2\pi i n v}{N}\right) \quad \text{for} \quad 0 \le v < N.. \tag{70}$$

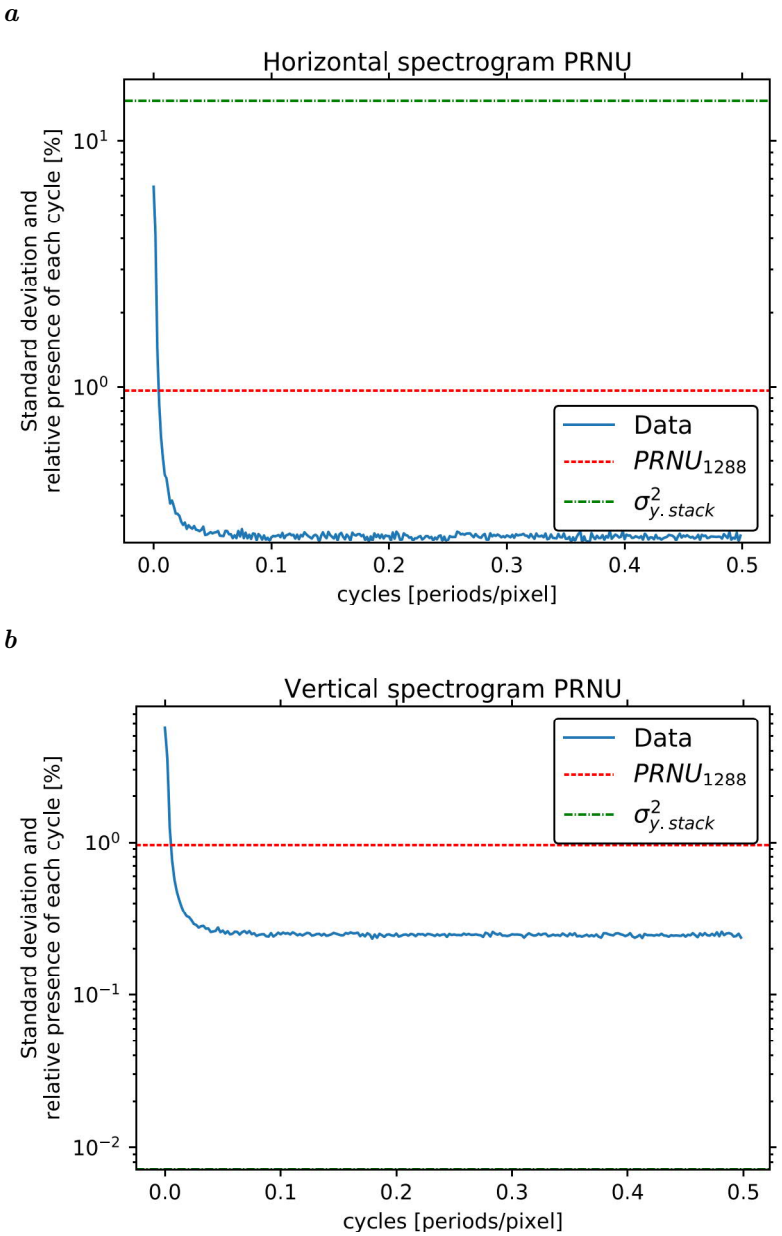

Figure 13: *Example for spectrograms of the photoresponse:* ***a*** *horizontal spectrogram,* ***b*** *vertical spectrogram, together with a two horizontal lines: One marks the white noise spectrum corresponding to the standard deviation of the temporal noise $\sigma_{y.stack}$ in percent for acquiring a single image without averaging and the second the PRNU. A comparison of the spectrogram with the PRNU reveals how much peaks in the spectrogram contribute to the PRNU.*

3. Compute the mean power spectrum $p[v]$ averaged over all M row spectra:

$$P[v] = \frac{1}{M}\sum_{m=0}^{M-1} \hat{y}[m][v]\hat{y}^*[m][v], \tag{71}$$

where the superscript $*$ denotes the complex conjugate. The power spectrum according to Eq. (71) is scaled in such a way that white noise gets a flat spectrum with a mean value corresponding to the spatial variance s_y^2.

In the spectrograms the square root of the power spectrum, $\sqrt{p[v]}$, is displayed as a function of the spatial frequency v/N (in units of cycles per pixel) up to $v = N/2$ (Nyquist frequency). It is sufficient to draw only the first part of the power spectrum

because the power spectrum has an even symmetry

$$P[N-v] = P[v] \quad \forall v \in [1, N/2].$$

In these plots the level of the white noise corresponds directly to the standard deviation of the spatial white noise. Please note that the peak height in the spectrograms are not equal to the amplitude of corresponding periodic patterns. The amplitude a of a periodic pattern can be computed by adding up the spatial frequencies in the power spectrum belonging to a peak:

$$a = 2\left(\frac{1}{N}\sum_{v_{\min}}^{v_{\max}} P[v]\right)^{1/2}. \tag{72}$$

For the vertical spectrograms (area cameras only), the same computations are performed (Fig. 12b and Fig. 13b). Only rows and columns must be interchanged.

4. Add a line with the DSNU_{1288} Eq. (66) and PRNU_{1288} Eq. (67) to the corresponding spectrogram plots (Figs. 12 and 13). Because the PRNU is given as a relative value to the mean value (Eq. (67)), also the spectrogram values and the temporal noise (see next item) must be divided by the mean values.
5. Also add a line with the standard deviation of the temporal noise, $\sigma_{y.\text{stack}}$ according to Eq. (65) (Figs. 12 and 13). In this way, it is easy to compare spatial and temporal noise.

8.7 Horizontal and Vertical Profiles

The spatial nonuniformities are further illustrated by plots of horizontal and vertical profiles of the none highpass-filtered (compare Section 8.1) DSNU and PRNU — in total four plots. Each plot contains four profiles (Example Fig. 14)

middle: Horizontal row $M/2$ (vertical profile of column $N/2$) through the center of the image. The correct row/column number is given by integer arithmetics, i. e., the largest integer smaller than the half value; indices start with 0.

mean: Average of all rows (all columns).

max: Maximum of all rows (all columns) at each horizontal (vertical) position. These profiles nicely show even only few pixels with positive outliers, e. g. hot pixels in the DSNU image.

min: Minimum of all rows (all columns) at each horizontal (vertical) position. These profiles nicely show even only few pixels with negative outliers, e. g. less sensitive pixels in the PRNU image.

The profiles are directly computed from the averaged dark image $\langle \boldsymbol{y}_{\text{dark}} \rangle$ and the PRNU image $\langle \boldsymbol{y}_{50} \rangle - \langle \boldsymbol{y}_{\text{dark}} \rangle$ defined in Section 4.2 without applying any corrections such as high-pass filtering.

The ranges of the profiles are set as follows:

DSNU profiles Take 0.9 times average of minimum line as lower limit and 1.1 times of average of maximum line as upper limit,

PRNU profiles Take 0.9 times average of mean value as lower limit and 1.1 times of average of mean value as upper limit. For PRNU profiles measured with a lens/camera combination take a range from zero to the maximum.

Label axes of both DSNU and PRNU profiles with units DN.

8.8 Defect Pixel Characterization

The computation of the logarithmic histogram involves the following computing steps for every averaged and highpass-filtered nonuniformity image $\boldsymbol{y}$. The following procedure is suggested to obtain optimally smooth histograms. It is based on the simple fact that nonuniformity images are averaged over L integer-valued images. Therefore their values are integer multiples of $1/L$ and the optimum interval width is therefore also an integer multiple of L.

1. Compute minimum and maximum values $y_{\min}$ and $y_{\max}$ of the image $\boldsymbol{y}$.

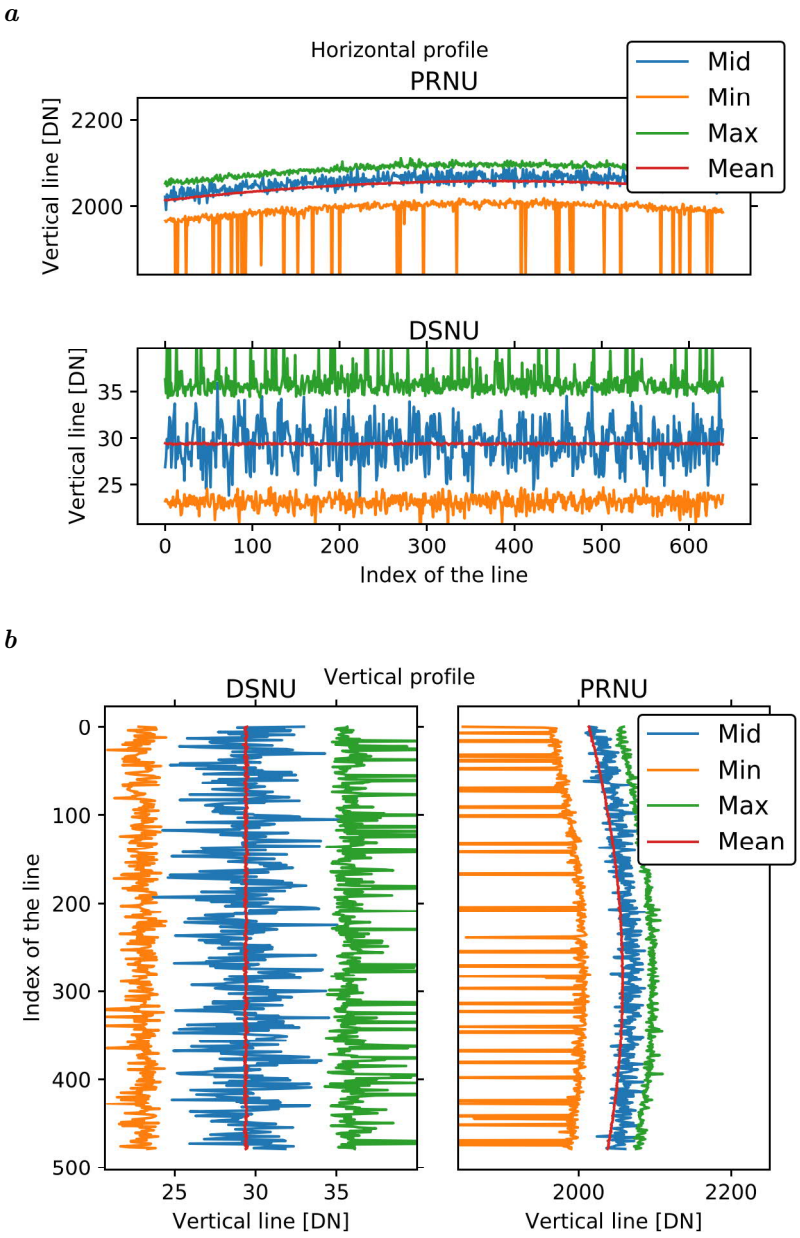

Figure 14: *Example for profile images:* ***a*** *horizontal profiles* ***b*** *vertical profiles.*

2. Part the interval between $y_{\min}$ and $y_{\max}$ into $Q = L(y_{\max} - y_{\min})/I + 1$ bins of equal width with the optimal bin width of I/L. Choose an appropriate $(I = 1, 2, 3, \ldots)$ so that the number of bins is lower than or equal to 256. This condition is met by

$$I = \text{floor}\left[\frac{L(y_{\max} - y_{\min})}{256}\right] + 1. \tag{73}$$

3. Compute a histogram with all values of the image using these bins. The bin q to be incremented for a value y is

$$q = \text{floor}\left[\frac{L(y - y_{\min})}{I}\right]. \tag{74}$$

In this way the Q bins of the histogram (indices from 0 to $Q-1$) cover values from $y_{\min}$ to $y_{\max} + (I-1)/L$
The values of the center of the bins as a deviation from the mean value are given as:

$$y[q] = y_{\min} + \frac{I-1}{2L} + q\frac{I}{L}. \tag{75}$$

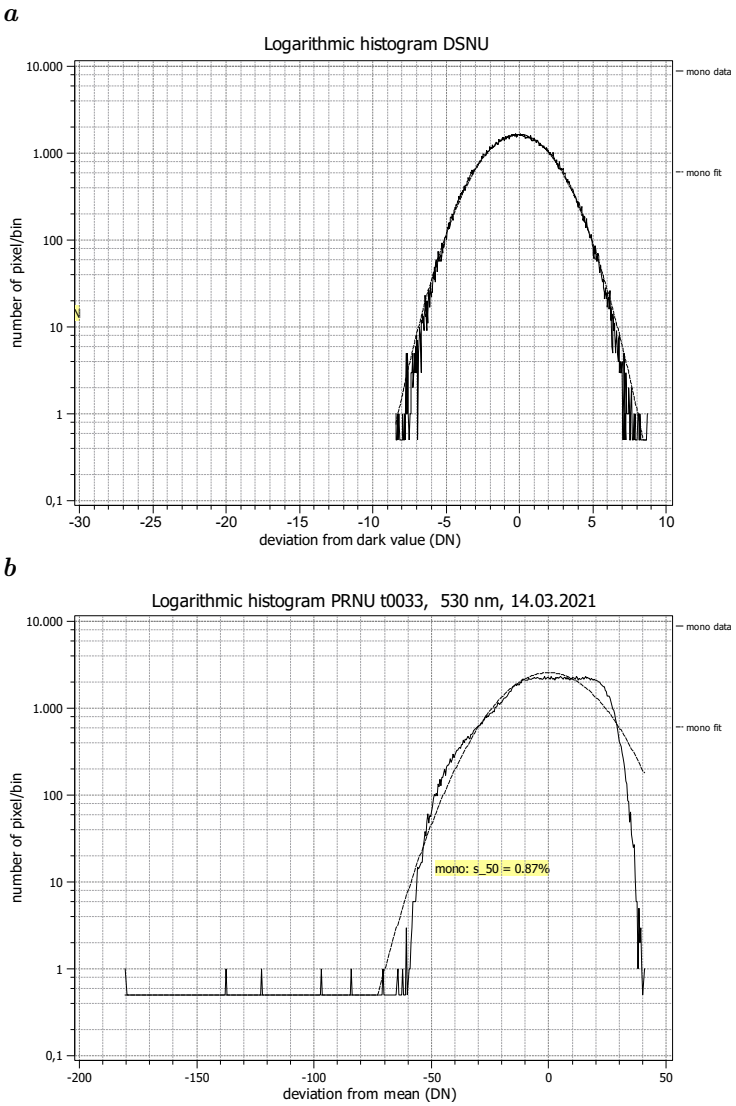

Figure 15: *Example for logarithmic histograms for* **a** *dark signal nonuniformity (DSNU),* **b** *photoresponse nonuniformity (PRNU). The dashed line is the model normal probability density distribution with the non-white standard deviation s_{nw} according to Eq. (76).*

4. Draw the histogram in a semilogarithmic plot. Use an x-axis with the values of the bins relative to the mean value. The y axis must start below 1 so that single outlying pixels can be observed.
5. Add the normal probability density distribution corresponding to the non-white variance s_{nw}^2 as a dashed line to the graph obtained for an $M \times N$ image with an interval width I/L:

$$p_{\text{normal}}[q] = \frac{I}{L} \cdot \frac{NM}{\sqrt{2\pi}\, s_{nw}} \cdot \exp\left(-\frac{y[q]^2}{2s_{nw}^2}\right). \tag{76}$$

The accumulated logarithmic histogram gives the probability distribution (integral of the probability density function) of the absolute deviation from the mean value. Thus the accumulated logarithmic histogram gives the number of pixels that show at least a certain absolute deviation from the mean in relation to the absolute deviation. The computation involves the following steps:

1. Subtract the mean from the nonuniformity image $\boldsymbol{y}$ and take the absolute value:

$$\boldsymbol{y}' = |\boldsymbol{y} - \mu_y| \tag{77}$$

2. Compute the maximum value $y'_{\max}$ of $\boldsymbol{y}'$; the minimum is zero. The rest of the compu-

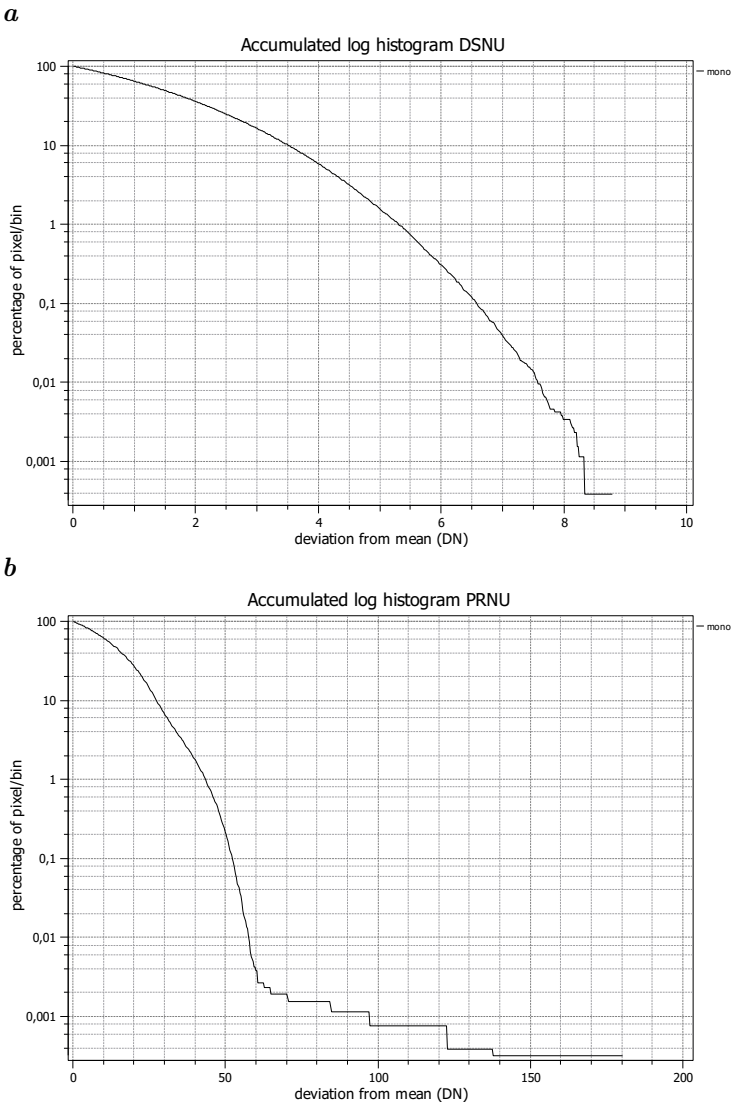

Figure 16: *Example for accumulated logarithmic histograms for* **a** *dark signal nonuniformity (DSNU),* **b** *photoresponse nonuniformity (PRNU).*

tation is equivalent to the computation of the non-accumulated histograms of above if $y_{\min}$ is replaced by zero and $y_{\max}$ by $y'_{\max}$.

3. Part the interval between 0 and $y'_{\max}$ into $Q = L\,y'_{\max}/I + 1$ bins of equal width with the optimal bin width of I/L. Choose an appropriate $(I = 1, 2, 3, \ldots)$ so that the number of bins is lower than or equal to 256. This condition is met by

$$I = \text{floor}\left[\frac{L\,y'_{\max}}{256}\right] + 1. \tag{78}$$

4. Compute a histogram with all values of the image using these bins. The bin q to be incremented for a value y is

$$q = \text{floor}\left(Ly'/I\right). \tag{79}$$

The values of the center of the bins as a deviation from the mean value are given as:

$$y'[q] = \frac{I-1}{2L} + q\frac{I}{L}. \tag{80}$$

5. Accumulate the histogram. If $h[q']$ are the Q values of the histogram, then the values of

the accumulated histogram $H[q]$ are:

$$H[q] = \sum_{q'=q}^{Q} h[q']. \tag{81}$$

6. Draw the accumulated histogram $H[q]$ as a function of $y'[q]$ in a semilogarithmic plot. Use a x-axis with the values of the bins relative to the mean value. The y axis must start below 1 so that single outlying pixels can be observed.

Logarithmic histograms and accumulated logarithmic histograms are computed and drawn for both the DSNU and the PRNU. This gives four graphs in total as shown in Figs. 15 and 16.

9 Methods for Spectral Sensitivity

9.1 Spectral Light Source Setup

The measurement of the spectral dependence of the quantum efficiency requires a separate experimental setup with a light source that can be scanned over a certain wavelength range. This apparatus includes either a monochromator with a broadband light source or a light source that can be switched between different wavelengths by any other means. Use an appropriate optical setup to ensure that the light source has the same geometrical properties as detailed in Section 6.1. This means that a light source with a diameter D must evenly illuminate the sensor array or calibration photodiode placed at a distance $d = 8D$ with a diameter $D' \leq D$. A different aperture d/D can be used and must be reported. It is advantageous to set up the whole system in such a way that the photon irradiance is about the same for all wavelengths.

Spectroscopic measurements are quite demanding. It might not be possible to irradiate the whole sensor evenly. Therefore only a section of the sensor may be used for the spectroscopic measurements.

9.2 Measuring Conditions

This section summarizes the measuring conditions.

Sensor area. Specify the fraction of the sensor area used (all, half, ...).

Operation point. The operation point must be the same as for all other measurements.

Bandwidth. The FWHM (full width at half maximum) bandwidth of the light source shall be less than 10 nm. If it is technically not feasible to work with such narrow FWHM, the FWHM bandwidth can be enlarged to values up to 50 nm. The FWHM used for the measurement must be reported. Please note that if you use a FWHM larger than 10 nm it will not be possible to evaluate the color rendition of a color sensor, e. g., according to the ISO 13655 and CIE 15.2. Some image sensors show significant oscillations in the quantum efficiency as a function of the wavelength of the light (Fig. 17). If such oscillations occur, the peak positions vary from sensor to sensor. Therefore it is allowed to smooth, provided that the filter procedure is described including the width of the filter.

Wavelength range. The scanned wavelength range should cover all wavelength to which the sensor responds. Normally, this includes a wavelength range from at least 350 nm to 1100 nm. For UV sensitive sensors the wavelength range must be extended to correspondingly shorter wavelengths, typically down to 200 nm. If technically feasible, the number of measuring points must be chosen in such a way that the whole wavelength range is covered without gaps. This implies that the distance between neighboring wavelengths is smaller than or equal to the 2 FWHM.

Signal range. An exposure time should be set to a value so that sufficiently large signals are obtained for all wavelengths. If the radiance of the light source shows large variations for different wavelengths, this could require more than one spectral scan with different exposure times. Before and after each wavelength sweep and for every exposure time used, a dark image must be taken.

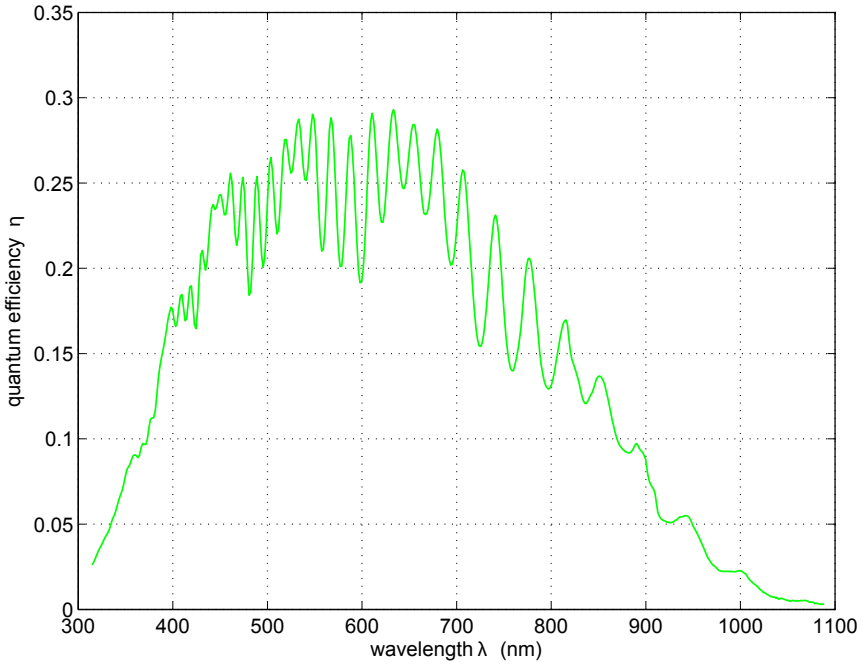

Figure 17: *Example for a spectroscopic measurement of the quantum efficiency in a range from 300–1100 nm with a FWHM of 10 nm, no smoothing is applied.*

9.3 Calibration

The experimental setup is calibrated in the same way as the monochromatic setup (Section 6.4). The image sensor is replaced by a calibrated photodiode for these measurements. From the measured irradiance at the sensor surface, the number of photons $\mu_p(\lambda)$ collected during the exposure time are computed using Eq. (3).

9.4 Evaluation

The measured wavelength dependent quantum efficiency is averaged over all pixels of the sensor or the selected sensor area. For color cameras, the spectral response must be evaluated for all colors separately just in the same way as described at the end of Section 6.6.

The evaluation procedure contains the following steps for every chosen wavelength:

1. Compute the mean spectral gray value.
2. Subtract the mean dark value from the mean spectral values.
3. Divide by K, as determined from the linearity and sensitivity measurements (Section 6.6), performed at the *same* operation point, to compute the number of accumulated charge units.
4. Divide by the mean number of photons, $\mu_p(\lambda)$, calculated using the spectral calibration curve Section 9.3 to obtain the quantum efficiency:

$$\eta(\lambda) = \frac{\mu_y(\lambda) - \mu_y.\text{dark}}{K\,\mu_p(\lambda)}. \tag{82}$$

An example curve is shown in Fig. 17.

10 Publishing the Results

This section describes the basic information which must be published for each camera and precedes the EMVA 1288 data.

10.1 Basic Information

Item	Description
Vendor	Name
Model	Name
Type of data presented[1]	Single; typical; guaranteed; guaranteed over life time
Sensor type	CCD, CMOS, CID, ...
Sensor diagonal	in [mm] (Sensor length in the case of line sensors)
Lens category	Indication of lens category required [inch]
Resolution	Resolution of the sensor's active area: width x height in [pixels]
Pixel size	width x height in [μm]
CCD only	
Readout type	progressive scan or interlaced
Transfer type	interline transfer, frame transfer, full frame transfer, frame interline transfer
CMOS only	
Shutter type	Global: all pixels start exposing and stop exposing at the same time. Rolling: exposure starts line by line with a slight delay between line starts; the exposure time for each line is the same. Other: defined in the datasheet.
Overlap capabilities	Overlapping: readout of frame n and exposure of frame n+1 can happen at the same time. Non-overlapping: readout of frame n and exposure of frame n+1 can only happen sequentially. Other: defined in the datasheet.
Maximum readout rate	number of frames per second (or lines per second for line sensors) at the given operation point (no change of settings permitted)
Dark current compensation	Specify whether camera has dark current compensation
Interface type	Analog[2], any of the interface standards (GigE, USB Vision, CoaxPress, ...) or proprietary
Operation point(s)	Describe operation points used for EMVA 1288 measurements (including gain, offset, maximum exposure time, mode of camera, ...). Must include all parameter so that everybody reading the datasheet can repeat the measurements. Parameters not given are assumed to be factory default.
EMVA 1288	Specify which test equipment, which release of the EMVA 1288 standard was used and which optional EMVA 1288 data have been measured

[1]Specify definition used for typical data, e. g., number of samples, sample selection. The type of data may vary for different parameters, e. g., guaranteed specification for most of the parameters and typical data for some measurements not easily done in production. It then has to be clearly indicated which data is of what nature.

[2] Specify frame grabber used with analog camera

10.2 The EMVA 1288 Datasheet

The data sheet is structured in the following way:

Optional cover page Free for anything. Typical first page from companies (key features, description, picture, etc). Any layout is possible. If present, the first page must contain the EMVA1288 logo.

Table 2: *List of all EMVA 1288 parameters*

Type of measurement	Reference
Quantum efficiency η	in %
Gain K	units DN/e$^-$
Gain $1/K$	units e$^-$/DN
Dark noise	in units DN
	in units e$^-$
Signal to noise ratio $\mathrm{SNR}_{\max}$	as ratio
	in units dB
$\mathrm{SNR}_{\max}^{-1}$	in %
Absolute sensitivity threshold	in number of electrons
	in number of electrons per μm^2
Saturation capacity	in number of electrons
	in number of electrons per μm^2
Dynamic range (DR)	as ratio
	in units dB
DSNU_{1288}	in units e$^-$
$\mathrm{DSNU}_{1288.\mathrm{row}}$	in units e$^-$
$\mathrm{DSNU}_{1288\mathrm{col}}$	in units e$^-$
$\mathrm{DSNU}_{1288.\mathrm{pix}}$	in units e$^-$
PRNU_{1288}	in %
$\mathrm{PRNU}_{1288.\mathrm{row}}$	in %
$\mathrm{PRNU}_{1288.\mathrm{col}}$	in %
$\mathrm{PRNU}_{1288.\mathrm{pix}}$	in %
Non-linearity error LE	%
Dark current from mean	in units e$^-$/s
Dark current from variance	in units e$^-$/s

General One or more pages describing the test equipment used, the version of the EMVA 1288 standard used, the basic camera parameters and a summary of the operation points for which measurements are provided (see first page of attached document). If spectrometric measurements are performed, a graph with the wavelength dependency of the quantum efficiency (Fig. 17) is included. The date when the measurement was performed must be provided on request.

Summary page for each operating point Each page is a summary of the results for one of the operating points (see second page of attached document). The summary page contains a description of the operating point, a graph with the photon transfer curve (Fig. 7), a graph with the SNR curve (Fig. 8) and a one-column table with all quantities according to Table 2, which are detailed in Sections 6–9. The header contains the EMVA 1288 logo on the left and the company logo on the right.

Detailed results for each operating point For each operating point more specific details about the test conditions, large size plots, and for each plot a table with the extracted data.

A template of the summary data sheet is published together with this release in a separate document. It clearly specifies which graphs and camera parameter must be placed where in the data sheet. It also details all the axes labeling of the graphs.

A Bibliography

[1] Aster, R. C., Borchers, B., and Thurber, C. H.: Parameter Estimation and Inverse Problems, vol. 90 of *International Geophysics Series*, Academic Press, Boston, 2 edn., doi: 10.1016/B978-0-12-385048-5.00030-6, URL https://sites.warnercnr.colostate.edu/aster/2014/07/24/parameter-estimation-and-inverse-problems/, 2013.

[2] Darmont, A.: High Dynamic Range Imaging: Sensors and Architectures, SPIE, 2 edn., doi: 10.1117/3.2512264, 2019.

[3] Darmont, A., Chahiba, J., Lemaitre, J. F., Pirson, M., and Dethier, D.: Implementing and using the EMVA1288 standard, in: Sensors, Cameras, and Systems for Industrial/Scientific Applications XIII, edited by Widenhorn, R., Nguyen, V., and Dupret, A., vol. 8298 of *Proc. SPIE*, p. 82980H, doi: 10.1117/12.905874, 2012.

[4] Denvir, D. J. and Conroy, E.: Electron multiplying CCDs, in: Optical Metrology, Imaging, and Machine Vision, edited by Shearer, A., Murtagh, F. D., Mahon, J., and Whelan, P. F., vol. 4877 of *SPIE Proc.*, pp. 55–68, 2003.

[5] DeWeert, M. J., Cole, J. B., Sparks, A. W., and Acker, A.: Photon transfer methods and results for electron multiplication CCDs, in: Applications of Digital Image Processing XXVII, edited by Tescher, A. G., vol. 5558 of *SPIE Proc.*, pp. 248–259, 2004.

[6] Dierks, F.: Sensitivity and Image Quality of Digital Cameras, Tech. rep., Basler AG, 2004.

[7] Dittrich, P.-G., Bichra, M., Pfützenreuter, C., Rosenberger, M., and Notni, G.: Measurement principle and arrangement for the determination of spectral channel-specific angle dependencies for multispectral resolving filter-on-chip CMOS cameras, in: Photonics and Education in Measurement Science 2019, edited by Rosenberger, M., Dittrich, P.-G., and Zagar, B., vol. 11144, pp. 180–190, International Society for Optics and Photonics, SPIE, doi: 10.1117/12.2527871, 2019.

[8] Dittrich, P.-G., Bichra, M., Stiehler, D., Pfützenreuter, C., Radtke, L., Rosenberger, M., and Notni, G.: Extended characterization of multispectral resolving filter-on-chip snapshot-mosaic CMOS cameras, in: Algorithms, Technologies, and Applications for Multispectral and Hyperspectral Imagery XXV, edited by Velez-Reyes, M. and Messinger, D. W., vol. 10986, pp. 140–150, International Society for Optics and Photonics, SPIE, doi: 10.1117/12.2518842, 2019.

[9] Dittrich, P.-G., Rosenberger, M., and Notni, G.: Measurement, comparison, and evaluation of spectral sensitivity curves from different multispectral resolving snapshot-mosaic cameras, in: Algorithms, Technologies, and Applications for Multispectral and Hyperspectral Imagery XXVI, edited by Velez-Reyes, M. and Messinger, D. W., vol. 11392, International Society for Optics and Photonics, SPIE, doi: 10.1117/12.2564690, 2020.

[10] EMVA 1288 Working Group: EMVA Standard 1288 - Standard for Characterization of Image Sensors and Cameras, Release A2.01, open standard, European Machine Vision Association, doi: 10.5281/zenodo.1402251, 2007.

[11] EMVA 1288 Working Group: EMVA Standard 1288 - Standard for Characterization of Image Sensors and Cameras, Release 3.0, open standard, European Machine Vision Association, doi: 10.5281/zenodo.10696, 2010.

[12] EMVA 1288 Working Group: EMVA Standard 1288 - Standard for Characterization of Image Sensors and Cameras, Release 3.1, open standard, European Machine Vision Association, doi: 10.5281/zenodo.235942, 2016.

[13] Holst, G. C. and Lomheim, T. S.: CMOS/CCD Sensors and Camera Systems, SPIE Press, Bellingham, Washington, USA, 2 edn., 2011.

[14] Janesick, J., Klaasen, K., and Elliott, T.: CCD charge collection efficiency and the photon transfer technique, in: Solid State Imaging Arrays, edited by Dereniak, E. L. and Prettyjohns, K. N., vol. 570, pp. 7–19, Proc. SPIE, doi: 10.1117/12.950297, 1985.

[15] Janesick, J. R.: Scientific Charge-Coupled Devices, SPIE, Bellingham, WA, doi: 10.1117/3.374903, 2001.

[16] Janesick, J. R.: Photon Transfer, SPIE Press, doi: 10.1117/3.725073, 2007.

[17] Jähne, B.: Digital Image Processing, Springer, Berlin, 6 edn., doi: 10.1007/3-540-27563-0, 2005.

[18] Jähne, B.: Release 4 of the EMVA 1288 standard: adaption and extension to modern image sensors, in: Forum Bildverarbeitung, edited by Heizmann, M. and Längle, T., pp. 13–24, KIT Scientific Publishing, doi: 10.5445/KSP/1000124383, 2020.

[19] Labsphere: A Guide to Integrating Sphere Theory and Applications, technical guide, see http://www.labsphere.com/, 2003.

[20] Labsphere: Integrating Sphere Uniform Light Source Applications, technical guide, see http://www.labsphere.com/, 2003.

[21] Montgomery, D. C., Peck, E. A., and Vining, G. G.: Introduction to Linear Regression Analysis, John Wiley & Sons, 5 edn., URL http://eu.wiley.com/WileyCDA/WileyTitle/productCd-0470542810.html, 2012.

[22] Papoulis, A.: Probability, Random Variables and Stochastic Processes, McGraw-Hill, 3 edn., 1991.

[23] Radtke, L., Graf-Batuchtin, I., Rosenberger, M., and Notni, G.: Adaptive test bench for characterizing image processing sensors, in: Image Sensing Technologies: Materials, Devices, Systems, and Applications V, vol. 10656 of *Proc. SPIE*, doi: 10.1117/12.2304874, 2018.

[24] Rebhan, D., Dittrich, P.-G., Rosenberger, M., and Notni, G.: Radiometric extension of a measurement arrangement in accordance with the EMVA 1288 standard for camera characterization in UV to NIR wavelength range, Journal of Physics: Conference Series, 1379, 012 056, doi: 10.1088/1742-6596/1379/1/012056, 2019.

[25] Rosenberger, M., Zhang, C., Votyakov, P., Preißler, M., Celestre, R., and Notni, G.: EMVA 1288 camera characterisation and the influences of radiometric camera characteristics on geometric measurements, Acta IMEKO, 5, 81–87, doi: 10.21014/acta_imeko.v5i4.356, 2016.

[26] Saleh, B. and Teich, M.: Fundamentals of Photonics, Wiley-Interscience, 2 edn., doi: 10.1002/0471213748, 2007.

[27] Theuwissen, A. J. P.: Solid-State Imaging with Charge-Coupled Devices, Kluwer Academic Publishers, doi: 10.1007/0-306-47119-1, 1995.

[28] Widrow, B. and Kollar, I.: Quantization Noise — Roundoff Error in Digital Computation, Signal Processing, Control, and Communications, Cambridge Univ Press, URL www.cambridge.org/9780521886710, 2008.

B Notation

This section summarizes the used notation in two tables. The first table describes all quantities used, the second table, the meaning of indices that are used with various quantities. With this split in the description, the notation tables are much shorter.

Quantity	Units	Description
A	μm^2	Area of a sensor element (pixel)
c	m/s	Velocity of light
d	mm	Distance of sensor plane to opening (aperture) of light source
D	mm	Diameter of opening (aperture) of light source
D'	mm	Diameter of image sensor
DSNU_{1288}	DN	Dark signal nonuniformity
DR	1, dB, bits	Dynamic range
E	W/m^2, Photons/(s pixel)	Irradiance and quantum irradiance at sensor plane
h	Js	Planck constant
H	Ws/m^2, Photons/pixel	Radiant and quantum exposure at sensor plane
k	m^{-1}	wave number
K	DN/e^-	Overall system gain of a digital camera
PRNU_{1288}	%	Photo response nonuniformity
SNR	1, dB, bits	Signal-to-noise ratio
$\boldsymbol{P}$	—	Power spectrum
R	DN/p	Responsivity (slope characteristic curve)
s	—	*spatial* standard deviation of the quantity put into the index
s^2	—	*spatial* variance of the quantity put into the index
$\boldsymbol{s}$	DN	Digital image sequence
t_{exp}	s	Exposure time
y	DN	Digital gray value
$\boldsymbol{y}$	DN	2-D digital image
η	1	Total quantum efficiency, def. Eq. (2)
λ	nm	wavelength of light
μ	—	mean of the quantity put into the index
ν	Hz	frequency of light
σ	—	*temporal* standard deviation of the quantity put into the index
σ^2	—	*temporal* variance of the quantity put into the index

Index	Units	Description
d	e^-	relates to dark signal in units of e^-
dark	DN	relates to dark signal in units of DN
e	—	relates to number of electrons
min	—	relates to absolute sensitivity threshold
p	—	relates to number of photons
q	—	relates to quantization noise
sat	—	relates to saturation of the sensor
stack	—	relates to an image sequence (stack of images)
y	—	relates to a digital gray value
[l]	—	selection of image number l from an image sequence with L images, l runs from 0 to $L-1$
[m]	—	selection of a row in an image, m runs from 0 to $M-1$
[n]	—	selection of a column in an image, n runs from 0 to $N-1$

C Changes to Release A2.01

This section summarizes the changes of release 3.0 over the previous release A2.01 of the EMVA 1288 standard. Mostly, only extensions were added to the standard as described in Section C.1. To improve the standard and simplify its usage some minor changes were necessary. All these changes were implemented in release 3.0 in a way so that the data of cameras measured according to the specifications of release A2.01 are still valid.

C.1 Added Features

The following features are added to release 3.0 of the standard:

1. Color sensors and color cameras and not only gray scale cameras are now covered
2. Flexible characterization of defect pixels via logarithmic histograms (Sections 4.4 and 8)

C.2 Extension of Methods to Vary Irradiation

In release A2.01 of the standard, the photon transfer method (sensitivity and noise measurements) had to be performed with a continuous light source and varying exposure times, while the linearity measurements had to be measured with a constant exposure time and a pulsed light source with varying pulse widths. This was awkward, because the same type of measurements had to be performed twice.

With release 3.0 of the standard, any method described in Section 6.3 can be used to vary the radiant exposure and so the *same* set of measurements can be used to evaluate the data according to the photon transfer method (Section 6.6) and to determine the linearity error (Section 6).

C.3 Modifications in Conditions and Procedures

The following measuring conditions have been unified, described more precisely, or been changed:

1. For the photon transfer method, the mean value has to be computed from *both* images according to Eq. (16), and not only from the first as in release A2.01.
2. Condition to set the offset of the camera in order to avoid underflow with linearity measurements and nonuniformity measurements (Section 6.5). In release A2.01 different conditions were prescribed for linearity measurements, photo transfer measurements, and nonuniformity measurements.
3. The number of measuring points for sensitivity, linearity, and noise measurements is increased to 50. Only for production measurements as few as 9 values are allowed.

4. Number of images to be used for nonuniformity measurements. It is now possible to perform these measurements with just 16 images for inline inspection by correcting the bias caused by the residual temporal noise (Section 8).
5. The spatial noise is no longer contained in the definition of the SNR (compare Eq. (21) with Eq. 15 of release A2.01. This change has been made, because it is possible to reduce the spatial nonuniformities by suitable shading correction techniques with a single image, while this is not possible with the temporal noise.
6. The condition for the gray value range for the regression of the mean gray values against the exposure has been better adapted to possible nonlinearities in this relation. In release A2.01 it was at least the range from the dark image to 80% of the maximum temporal variance (Section 6.6), now it is reduced to 70%.
7. For a computation of the absolute sensitivity threshold the more accurate equation Eq. (26) is used. This change was required because the old equation without the correction term 1/2 in release A2.01 is not accurate enough for cameras with a very low dark noise of only a few electrons.
8. The linearity LE must be specified for the interval of 5–95% of the saturation points (Section 6.9).
9. For dark current measurements a minimum number of six equally spaced exposure times must be used (Section 7.1).
10. For a proper analysis of defect pixels, highpass filtering is introduced so that the PRNU measurements are not spoiled by the imperfections of the used light source (Section **??**). This highpass filtering is used also before *all* other nonuniformity evaluations including the estimation of spatial variances (Section 8.2) except for the computation of the spectrograms and all quantities derived from them (Section 8.6).
11. Measuring conditions for spectral measurements are relaxed (Section 9). The f-number can now deviate from 8, but must be reported.

C.4 Limit for Minimal Temporal Standard Deviation; Introduction of Quantization Noise

In the previous releases of the standard, quantization noise was neglected in the linear camera model. This led to a more complicated measuring procedure with low-resolution digitalization, i. e., 8 bit cameras. The problem resulted from the fact that the standard deviation of the temporal noise in the dark image may become smaller than the quantization interval.

Versions 1 and 2 of the EMVA 1288 standard therefore recommended:

> *"The gain setting of the camera is as small as possible but large enough to ensure that in darkness*
>
> $$K\sigma_d \geq 1$$
>
> *holds true (Otherwise, the quantization noise will spoil the measurement.)"*

It turns out that this limit is too cautious [28]. Monte-Carlo simulations were performed to check how accurate the mean and the variance can be estimated as a function of standard deviation σ_y in units DN. For the simulations 201 mean gray values equally distributed between 0 and 1 were taken and zero-mean normally distributed noise was added to the values. The estimated mean and variances were averaged over 900 000 realizations of each value. Finally, the deviations in the estimations were averaged over all 201 values.

The results are shown in the range $[0.3, 1]$ for σ_y in Fig. 18. The mean gray value can be estimated with a maximum error of less than 0.014 DN even for standard deviations as low as 0.4 DN (Fig. 18b). The estimate of the standard deviation is biased by the additional standard deviation of the quantization, $\sigma_q = \sqrt{1/12}$. However, if the estimate of the standard deviation is corrected for the additional effect of the standard deviation of the quantization error (unbiased estimation)

$$\sigma_y^2 = \sigma_{\text{est}}^2 - \sigma_q^2 = \sigma_{\text{est}}^2 - 1/12, \tag{83}$$

the maximum error of the estimate remains below 0.04 DN even for standard deviations as low as 0.4 DN. The variation in the estimation of the standard deviation comes from the

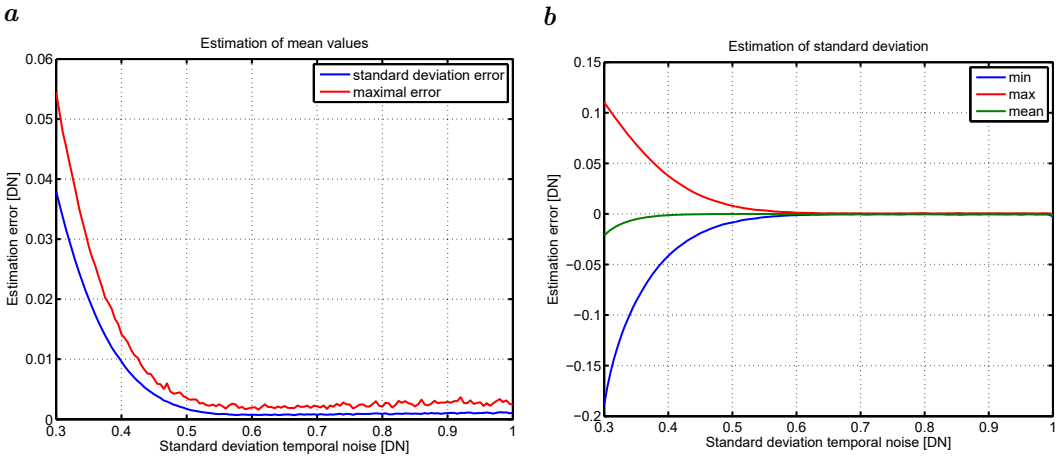

Figure 18: *Results from Monte Carlo simulations for the estimation of* **a** *the mean value and* **b** *the standard deviation of the digital gray value as a function of the standard deviation in units of digital numbers [DN] in the range between 0 and 1.*

different positions of the mean in the $[0, 1]$ interval. If it is close the edge of the interval, the values flip often either to the higher or lower value, resulting in a higher standard deviation. If the mean is in the middle of the interval this happens less frequently, so that the standard deviation is lower.

According to Eq. (18), the temporal noise is measured using the difference of two images. Therefore the temporal standard deviation of the difference image must be larger than $0.40\,\mathrm{DN}$ ... In conclusion, the variance $\sigma^2_{y.\mathrm{dark}}$ must be larger than $0.24\,\mathrm{DN}^2$. Subtracting the quantization noise variance $\sigma^2_q = 1/12\,\mathrm{DN}^2$, this results in a minimal detectable temporal standard deviation of $0.40\,\mathrm{DN}$. If the measured temporal variance is smaller than $0.24\,\mathrm{DN}^2$, two things can be stated:

1. The dynamic range is limited by the quantization noise (and the maximum possible but not determinable temporal noise to $\mu_{y.\mathrm{sat}}/0.49$.
2. The standard deviation of the dark noise in units e^- can be estimated to $\sigma_d < 0.40/K$.

The correction of the temporal noise by the quantization noise, which is possible down to a measured temporal noise variance of 0.24, expands the measurable dynamic range of a camera by a factor of about 2 over the condition of release A2.01. For a 8-bit camera, the maximum and measurable dynamic range is $255/0.49 \approx 500$

C.5 Highpass Filtering with Nonuniformity Measurements

The highpass filtering with defect pixel measurements is implemented by subtracting a 5×5 box-filtered image from the original mean images:

$$\boldsymbol{y}' = \boldsymbol{y} - {}^5\boldsymbol{R} * \boldsymbol{y} \quad \text{with} \quad {}^5R = \begin{bmatrix} 1 & 1 & 1 & 1 & 1 \\ 1 & 1 & 1 & 1 & 1 \\ 1 & 1 & 1 & 1 & 1 \\ 1 & 1 & 1 & 1 & 1 \\ 1 & 1 & 1 & 1 & 1 \end{bmatrix} /25. \tag{84}$$

The transfer function of this highpass filter is given by [17, p. 303]:

$${}^p\hat{h}(\tilde{k}_1, \tilde{k}_2) = 1 - \frac{\sin(\pi P \tilde{k}_1/2)}{P \sin(\pi \tilde{k}_1/2)} \cdot \frac{\sin(\pi P \tilde{k}_2/2)}{P \sin(\pi \tilde{k}_2/2)}, \tag{85}$$

where $P = 5$ and $\tilde{k}_1$ and $\tilde{k}_2$ are the wave numbers in horizontal and vertical direction, respectively, normalized by the spatial Nyquist frequency. This type of highpass filtering removes only a small fraction of the white noise. This can be computed by integrating over

the squared transfer function

$$s_{y'}^2 = s_y^2 \int_{\tilde{k}_1=0}^{1} \int_{\tilde{k}_2=0}^{1} \hat{r}^2(\tilde{k}_1, \tilde{k}_2)\, \mathrm{d}\tilde{k}_1 \mathrm{d}\tilde{k}_2 = s_y^2 (1 - r_{0,0})^2 = s_y^2 \left(1 - \frac{1}{P^2}\right)^2 = 0.92\, s_y^2, \tag{86}$$

provided that the spectrum of the random spatial variations is white (Section 4.1). Thus this method efficiently suppresses low-frequency spatial variations of the light source without reducing the estimate of the variance of the white noise significantly. For the proposed 5×5 box filter ($P = 5$), the reduction in the standard deviation is just 4%: $\sigma_{y'} = 0.96\, \sigma_y$. Therefore the measured spatial standard deviation $s_{y'}$ must be divided by 0.96 in order to obtain the correct value s_y.

For all further processing leave out two border lines at the top and bottom and two border columns on the left and right of the filtered image, because the filtering will not be exact in these areas. This procedure reduces the image size by four lines and four rows.

For line-scan cameras only a horizontal 5×1 box filter is applied. Therefore the correction factor is in this case (compare Eq. (86))

$$s_{y'}^2 = s_y^2 \int_{\tilde{k}_1=0}^{1} \hat{r}^2(\tilde{k}_1)\, \mathrm{d}\tilde{k}_1 = s_y^2 (1 - r_0)^2 = s_y^2 \left(1 - \frac{1}{P}\right)^2 = 0.64\, s_y^2. \tag{87}$$

The measured spatial standard deviation for line cameras $s_{y'}$ must be divided by 0.80 in order to obtain the correct value s_y. For all further processing of highpassed average nonuniformity images from line cameras leave out two border columns on the left and right.

D Changes to Release 3.0

This section summarizes the changes of release 3.1 over release 3.0 of the EMVA 1288 standard.

D.1 Changes

The changes include:

1. Spectral specification of light source (Section 6.2): Light source must also be specified by centroid wavelength λ_c. This wavelength should also be used instead of the peak wavelength λ_p for computation of the number of photons according to Eq. (3).
2. In some cases, just taking the maximum value of the variance in the photon transfer curve does not lead to a correct estimate of the saturation gray value (Section 6.6). Therefore the simple maximum search is replaced by a more sophisticated algorithm.
3. Changed algorithm to compute non-linearity: relative deviations are used instead of absolute deviation in order to account for the higher dynamic range of modern image sensors (Section 6.9).
4. The non-whiteness factor for the spatial variance of DSNU and PRNU (Section 8.6) is no longer reported, because the algorithms used in release 3.0 proved to be not reproducible enough to be a useful figure. If improved algorithms will be found in the future, the quantity will be incorporated again in an upcoming release.
5. Changed algorithm to compute bin width of logarithmic histograms for improving appearance of graphs without gaps (Section 8.8).

D.2 Added Features

The following features are added to release 3.1 of the standard:

1. Most importantly, release 3.1 now includes a template data sheet (Section 10.2)
2. Addition of total SNR: Definition is in Section 8.2, model curve according to Eq. (69) is added to SNR plot in Fig. 8.
3. Plots of horizontal and vertical profiles (Section 8.7).

E Changes to Release 3.1

E.1 Changes

1. Changed *license terms*, see page 1.
2. For the optional measurement of the temperature dependency of the dark current,the *doubling temperature* is no longer reported, because many modern sensors no longer show such a simple exponential increase. Only the data are reported (Sections 3.2 and 7.2)
3. Variation of expsoure: It is now possible to combine the three possible methods to vary the exposure in order to achieve a larger dynamic range of the exposure (Section 6.3).
4. Minor change in the computation of the variance of the temporal noise from two images (Section 6.6): It is now taken into account that the mean values of the two images taken at the same exposure might be slightly different. This change made it also possible to compute spatial variances from only two images (Section 4.2).
5. The *saturation gray value* $\mu_{y.\mathrm{sat}}$ (Section 6.6) is no longer defined by the maximum temporal variance in the photon transfer curve as in Release 3.1 but by negligible overflow in the distribution of the gray values. Extensive test runs showed that this change does not influence the values of the saturation capacity $\mu_{p.\mathrm{sat}}$ for a good linear camera but that it still gives good results if the photon transfer curve is disturbed.
6. For the computation of the absolute sensitivity threshold (Section 6.6) now the exact equation $\mu_p(\mathrm{SNR}=1)$, see Eq. (26), is used and no longer an approximation as in Release 3.1:

$$\frac{1}{\eta}\left(\sigma_{y.\mathrm{dark}}/K+\frac{1}{2}\right) \quad \text{replaced by} \quad \frac{1}{\eta}\left(\sqrt{\sigma_{y.\mathrm{dark}}^2/K^2+1/4}+\frac{1}{2}\right). \tag{88}$$

   This change was necessary, because the standard deviation of the temporal noise of modern image sensors is getting smaller and smaller.
7. More stable *linearity parameter*: The two linearity error parameters $\mathrm{LE}_{\min}$ and $\mathrm{LE}_{\max}$ of Release 3.1 are replaced by the single linearity error LE, describing the mean deviation from a linear regression (for details see Section 6.1).
8. Change in the correction of uneven illumination (Section 8.1)?
9. *Summary data sheet*: It must now contain the date of the measurement and the release used for the analysis (Release 3.1, Release 4.0 Linear or Release 4.0 General, ...) for a clear identification of which version of the standard has been used. The list of parameters no longer includes the optional doubling temperature for the dark current and some parameters that can easily be computed from the remaining parameters to make room for new parameters such as the more detailed description of nonuniformities (split into row, column, and pixel variations).

E.2 Added Features

1. *Extension of spectral range*: Release 4.0 Linear can now be applied from UV to SWIR, provided the conditions outlined in Section 1.2 are met, especially condition 6. Otherwise it is still possible to use Release 4.0 General.
2. Added analysis of *polarization parameters* and other derived parameters derived from multichannel sensors (Sections 2.3 and 6.8).
3. For all illumination steps not only the variance of the temporal noise is computed but also the variance of the *spatial nonuniformity*. Moreover, the latter is splitinto row, column, and pixel variations for a more detailed analysis of spatial nonuniformities. The SNR plot now also contains the measured *total SNR* for all data points (Section 4.3).
4. EMVA 1288 measurements can now also be performed optionally with *lens/camera combinations* (for details see Section 6.1).

E.3 Highpass Filtering with Nonuniformity Measurements

This section explains the improvements made with the highpass filtering of nonuniformity. The 5×5 box filter used in Release 3.1 (Appendix C.5) did a good job to suppress the

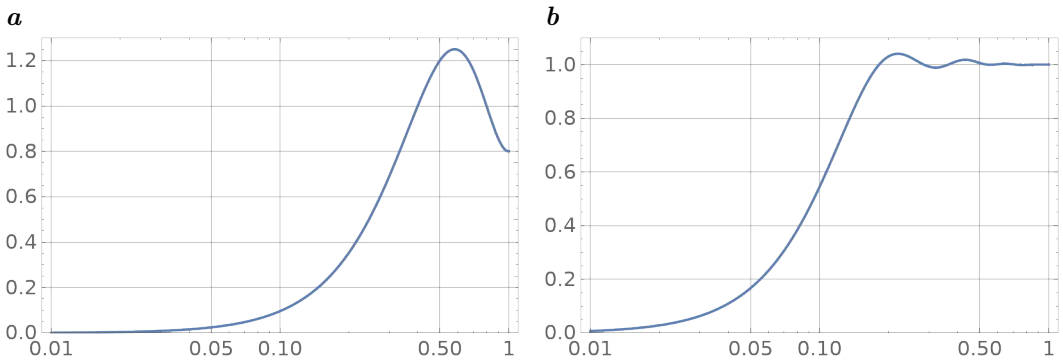

Figure 19: *Transfer function for highpass filtering of* ***a*** *Release 3.1 compared with the new highpass filter of* ***b*** *Release 4.0.*

low-frequency part, but does not preserve the high-frequency part very well. This can be shown by the transfer function for a high-pass filtering, when an image smoothed by a 5 × 5 box filter is subtracted from the original image. Because the box filter is separable, it is sufficient to show the transfer function of the one-dimensional 5 × 5 box filter. Fig. 19a shows the transfer function with wave numbers form 0.01 to 1 in a logarithmic scale (1 is the smallest possible wavelength with 2 pixels). While low frequencies are well suppressed, the amplitudes in the high-frequency deviate significantly from one. The transfer function should be one in this part, but it oscillates between 0.8 and 1.2. The highpass filter of Release 4.0 was optimized for a value close to one in the high-frequency part (Fig. 19b). The new highpass filter also preserves a much larger fraction of the high-frequency part down to structures with wavelengths as large as about 20 pixel.

F List of Contributors and History

EMVA gratefully acknowledges the active contributions to release 4.0 of this standard by the following members of the EMVA 1288 standardization committee, given in alphabetic order:

- Allied Vision Technologies GmbH, Stadtroda, Germany
- Basler AG, Ahrensburg, Germany
- Baumer Optronic GmbH, Radeberg, Germany
- FLIR Machine Vision, Richmond, Canada
- Gpixel nv, Antwerpen, Belgium
- HCI, Heidelberg University, Heidelberg, Germany
- Image Engineering GmbH & Co. KG, Köln, Germany
- JAI A/S, Copenhagen, Denmark
- Kaya Instruments, Nesher, Israel
- Labsphere, Inc., North Sutton, NH, USA
- LOOKLONG Imaging, Xi'an, China
- MATRIX VISION GmbH, Oppenweiler, Germany
- Matrox Electronic Systems Ltd., Dorval, Quebec, Canada
- PCO AG, Kelheim, Germany
- ON Semiconductor, Phoenix, Arizona, United States
- STEMMER IMAGING AG, Puchheim, Germany
- Technical University Ilmenau, Germany

The history of the EMVA 1288 dates back to 2004. The first meeting took place on February 2004 in Frankfurt, Germany. Among the initiators were Martin Wäny (Awaiba) and Fritz Dierks (Basler AG). Other major initial contributions came from Albert Theuwis-

sen (then Dalsa) and Emil Ott (PCO AG). The founding chair was Martin Wäny. Since 2008 the EMVA 1288 committee is chaired by Bernd Jähne (HCI, Heidelberg University).

A table of all releases of the EMVA standard 1288 concludes this document.

Date	Version	Document
August 2005	Release A1.00	https://doi.org/10.5281/zenodo.3951558
September 2006	Release A1.03	https://doi.org/10.5281/zenodo.1402249
August 2007	Release A2.01	https://doi.org/10.5281/zenodo.1402251
November 19, 2010	Release 3.0	https://doi.org/10.5281/zenodo.10696
December 30, 2016	Release 3.1	https://doi.org/10.5281/zenodo.235942
December 25, 2017	Chinese translation	https://doi.org/10.5281/zenodo.3541785
June 16, 2021	Release 4.0 Linear	**This document**
June 16, 2021	Release 4.0 General	**Available here**

G Template of Summary Data Sheet

See appended page.

Summary Sheet for Operation Point 1 at a Wavelength of 530 nm

Type of data	Single	Gain, black-level	0.0 dB, 5 DN
Exposure control	By irradiance	Environmental temperature	20.0°C
Exposure time	1.00 ms	Camera body temperature	29.0°C
Frame rate	100.0 Hz	Internal temperature(s)	—
Data transfer mode	Mono 12	Wavelength, centr., FWHM	530 nm, 30.0 nm

Photon Transfer

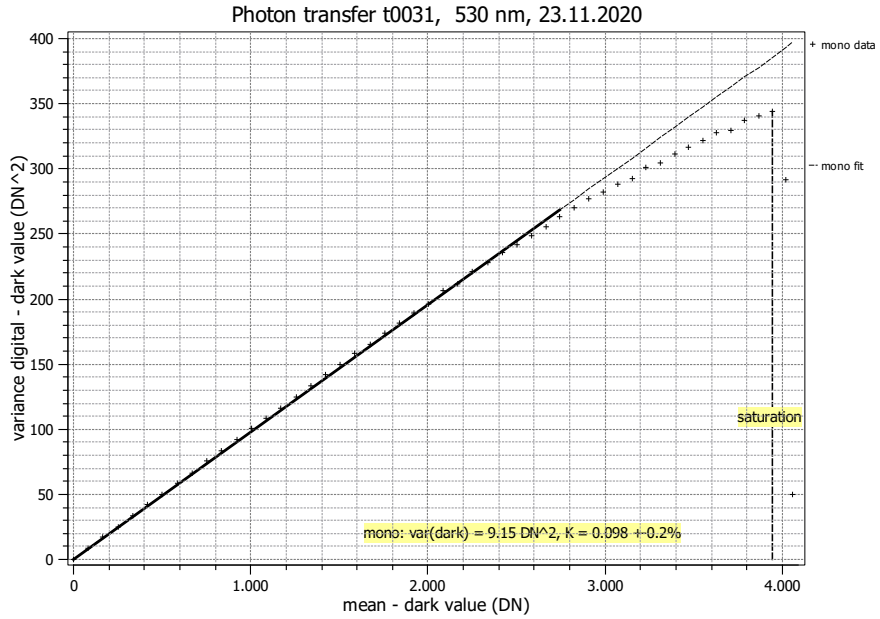

Signal-to-Noise Ratio

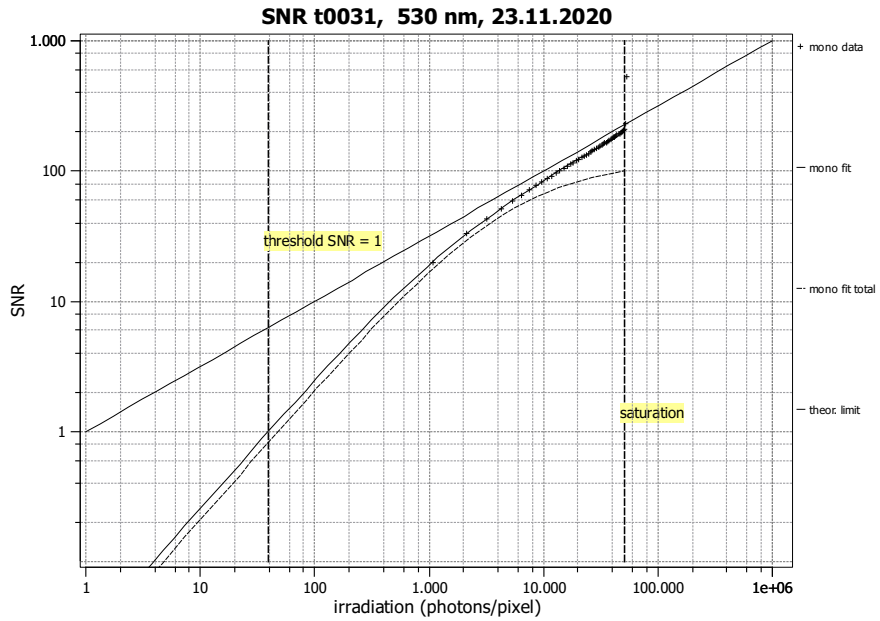

Quantum efficiency

η	79.4%

Overall system gain

K	0.098 DN/e$^-$
$1/K$	10.22 e$^-$/DN

Temporal dark noise

σ_d	30.8 e$^-$
$\sigma_{y.\mathrm{dark}}$	3.03 DN

Signal-to-noise ratio

$\mathrm{SNR}_{\max}$	202
	46.1 dB
$1/\mathrm{SNR}_{\max}$	0.49 %

Absolute sensitivity threshold

$\mu_{e.\mathrm{min}}$	31.4 e$^-$
$\mu_{e.\mathrm{min.area}}$	0.92 e$^-$/μm^2

Saturation capacity

$\mu_{e.\mathrm{sat}}$	40951 e$^-$
$\mu_{e.\mathrm{sat.area}}$	1193 e$^-$/μm^2

Dynamic range

DR	1303
	62.3 dB

Spatial nonuniformities

DSNU_{1288}	21.7 e$^-$
$\mathrm{DSNU}_{1288.\mathrm{col}}$	11.2 e$^-$
$\mathrm{DSNU}_{1288.\mathrm{row}}$	2.3 e$^-$
$\mathrm{DSNU}_{1288.\mathrm{pix}}$	18.4 e$^-$
PRNU_{1288}	0.87%
$\mathrm{PRNU}_{1288.\mathrm{col}}$	0.40%
$\mathrm{PRNU}_{1288.\mathrm{row}}$	0.21%
$\mathrm{PRNU}_{1288.\mathrm{pix}}$	0.74%

Linearity error

LE	0.36%

Dark current

$\mu_{c.\mathrm{mean}}$	5.1 ± 0.2 e$^-$/s
$\mu_{c.\mathrm{var}}$	5.2 ± 0.4 e$^-$/s